

GRI-03/0065 vol. 6

Seal Control of Hydrocarbon Migration and its Physical and Chemical Consequences

**VOLUME VI: A THEORETICAL ANALYSIS OF THE INORGANIC ALTERATION
BY THE FLOW OF BRINES THROUGH SEALS**

FINAL TECHNICAL REPORT
(6/19/1997-12/31/2001)

Prepared by:
J. Shosa and L. M. Cathles

Cornell University
Department of Earth & Atmospheric Sciences
Snee Hall
Ithaca, NY 14853

OSP #32006

Prepared for:

GAS RESEARCH INSTITUTE
5097-260-3787

December 2002

REPORT DOCUMENTATION PAGE

Form Approved
OMB No. 0704-0188

Public reporting burden for this collection of information is estimated to average 1 hour per response, including the time for reviewing instructions, searching data sources, gathering and maintaining the data needed, and completing and reviewing the collection of information. Send comments regarding this burden estimate or any other aspect of this collection of information, including suggestions for reducing this burden to Washington Headquarters Service, Directorate for Information Operations and Reports, 1215 Jefferson Davis Highway, Suite 1204, Arlington, VA 22202-4302, and to the Office of Management and Budget, Paperwork Reduction Project (0704-0188) Washington, DC 20503.

PLEASE DO NOT RETURN YOUR FORM TO THE ABOVE ADDRESS.

1. REPORT DATE (DD-MM-YYYY)			2. REPORT DATE		3. DATES COVERED (From - To)	
4. TITLE AND SUBTITLE				5a. CONTRACT NUMBER		
				5b. GRANT NUMBER		
				5c. PROGRAM ELEMENT NUMBER		
6. AUTHOR(S)				5d. PROJECT NUMBER		
				5e. TASK NUMBER		
				5f. WORK UNIT NUMBER		
7. PERFORMING ORGANIZATION NAME(S) AND ADDRESS(ES)					8. PERFORMING ORGANIZATION REPORT NUMBER	
9. SPONSORING/MONITORING AGENCY NAME(S) AND ADDRESS(ES)					10. SPONSOR/MONITOR'S ACRONYM(S)	
					11. SPONSORING/MONITORING AGENCY REPORT NUMBER GRI-03/0065 vol. 6	
12. DISTRIBUTION AVAILABILITY STATEMENT						
13. SUPPLEMENTARY NOTES						
14. ABSTRACT						
15. SUBJECT TERMS						
16. SECURITY CLASSIFICATION OF:			17. LIMITATION OF ABSTRACT	18. NUMBER OF PAGES	19a. NAME OF RESPONSIBLE PERSON	
a. REPORT	b. ABSTRACT	c. THIS PAGE			19b. TELEPHONE NUMBER (Include area code)	

GRI Disclaimer

LEGAL NOTICE

This report was prepared by Cornell University as an account of contracted work sponsored by the Gas Research Institute (GRI). Neither Cornell University, GRI, members of these companies, nor any person acting on their behalf:

- a. Makes any warranty or representation, expressed or implied, with respect to the accuracy, completeness, or usefulness of the information contained in this report, or that the use of any apparatus, methods, or process disclosed in this report may not infringe upon privately owned rights; or
- b. Assumes any liability with respect to the use of, or for damages resulting from the use of, any information, apparatus, method, or process disclosed in this report.

Table of Contents

GRI DISCLAIMER	3
TABLE OF CONTENTS	4
RESEARCH SUMMARY	5
VOLUME VI: A THEORETICAL ANALYSIS OF THE INORGANIC ALTERATION BY THE FLOW OF BRINES THROUGH SEALS	7
A. Abstract	7
B. Introduction	7
C. Theoretical Foundations	8
1. Alteration Caused by Brine Flow	8
2. The Buffered Chemical Composition of Basin Brines	10
3. Calculating Dissolution and Dissociation Log K.....	14
a. Equations of State for Minerals and Gases	15
b. Estimating Gibbs Free Energies of Silicate Minerals	16
c. Equations of State for Aqueous Species	17
d. Parameters for the HKF Equation of State	20
D. Simplified Estimation of the Revised-HKF Equation of State Coefficients ..	22
1. The Born Coefficient as a Function of Standard State Entropy and Charge	23
2. Reduction of a_i to a_1	23
3. Reduction of c_i to c_1	27
4. a_1 and c_1 as Functions of Standard State Entropy, Charge, and Species Type	29
E. Predicting Brine Chemistry	42
F. Inorganic Alteration by Brine Movement through Seals	42
1. P - T Gradients in Sedimentary Basins	42
2. Diagenetic Alteration	44
3. Flow Alteration in the Hydrostatic Zone	53
4. Alteration Due to Flow through Pressure Seals.....	54
5. Inorganic Alteration as a Function of Gas Saturation.....	59
6. Inorganic Alteration as a Function of Salinity.....	64
7. Estimating the Cumulative Fluid Flux as a Function of Intensity of Alteration...	65
8. Discussion	68
G. Acknowledgments	68
H. References	68

Research Summary

TITLE: A theoretical analysis of inorganic alteration by the flow of brines through seals

CONTRACTOR: Cornell University

PRINCIPAL INVESTIGATOR: Lawrence M. Cathles III

REPORT PERIOD: January 1, 1997 to December 31, 2001

OBJECTIVES: The objectives of this report are to:

- (1) develop a theoretical framework for predicting the inorganic alteration produced when brines are forced through basin seals, and
- (2) calculate the alteration produced by flow through seals under various hypothetical conditions.

TECHNICAL PERSPECTIVE: The interior of the northern offshore Gulf of Mexico Basin is divided into a complex system of variously over-pressured compartments. It is an area of active hydrocarbon generation and one of the world's most active areas of hydrocarbon exploration. There is no present consensus on how hydrocarbons migrate through these pressure compartments, the nature of the impermeable seals that separate the compartments, and how the flow of gas and brine affect hydrocarbon chemistry and inorganically alter sediments. One possibility is that both brine and hydrocarbon fluids are driven across seals when pressures increase to the point that the seals leak, and that brines and hydrocarbons move along common migration trajectories. This is a corollary of our capillary seal hypothesis. The movement of aqueous fluids through gradients of pressure, temperature, and salinity as they traverse seals causes inorganic alteration of the seal sediments. The intensity of this alteration is directly proportional to the amount of leakage. Thus seal alteration provides a map of where brines (and possibly hydrocarbons) have leaked through seals and a map of the brine (and possibly hydrocarbon) migration pathways in a basin.

RESULTS: Our calculations show that inorganic seal alteration is intense compared to diagenetic alteration, and that the mineralogy of the alteration potentially provides information on the steepness of pressure gradients in the seal and the mass fraction of gas in fluids that have crossed the seal.

**TECHNICAL
APPROACH:**

Conclusions are drawn by modeling the inorganic alteration caused by movements of different proportions of brine and gas through plausible pressure, temperature, and salinity gradients in seals. Local chemical equilibrium is assumed. A new, simplified, and potentially very powerful method of estimating the thermodynamic data needed to make the equilibrium chemical calculations is developed.

**PROJECT
IMPLICATIONS:**

Seals will be altered where they leak. The challenge is to map the pattern of alteration. The alteration is intense enough that it is possible it could be mapped seismically. Seismic alteration maps can be inverted using the methods presented here to yield quantitative maps of brine migration in a basin. The maps will show not only the migration pathways but also the amounts of brine that have traveled along those pathways. The new methods we have developed for estimating thermodynamic data could find very broad application.

**PROJECT
MANAGERS:**

Richard Parker and Robert Siegfried

Volume VI: A Theoretical Analysis of the Inorganic Alteration by the Flow of Brines through Seals

Lawrence M. Cathles III, Department of Earth and Atmospheric Sciences, Cornell University, Ithaca New York and Jennifer Shosa, Colby College, Waterville, Maine

A. Abstract

Brines and hydrocarbon fluids are driven across basin seals when sediment loading and hydrocarbon generation increases fluid pressure to the hydrofracture limit. Transiting a seal, the brines and hydrocarbons cross steep pressure gradients, elevated temperature gradients, and possibly salinity gradients. Since basin fluids are in equilibrium with sediment minerals, and since the solubility of these minerals is a function of pressure, temperature, and salinity, the movement of brines through pressure, temperature, and salinity gradients will cause mineral alteration of the sediments.

This report lays a theoretical foundation for calculating alteration due to the flow of brine and gas through seals. A new simplified method for estimating the dissolution log K of aqueous complexes is developed. The theory and parameter estimation methods are then used to calculate the mineral alteration that should occur in a variety of hypothetical seals. We show that the steep pressure gradients expected in capillary seals could, depending on the mineral buffer, produce alteration diagnostic of the existence of these seals. Increasing salinity increases alteration intensity more than proportionately. The passage of gas (as well as water) through a seal changes the alteration mineralogy in characteristic ways. The passage of 200 kg/cm² of brine through a seal at 3 km depth will cause >1 wt% of new minerals to precipitate. If brine flow is focused to particular discharge points on a minibasin scale, as the hydrocarbon flux analysis in Volume V of this series suggests, inorganic alteration at these locations should be as complete as exhaustion of the mineral buffer will allow.

We show theoretically and illustrate with examples how alteration can be interpreted in terms of total fluid throughput. The value of these methods to hydrocarbon exploration could be large because they could produce a quantitative map of fluid flow in a basin. The value of the methods depends on the ability to map basin alteration, and could be best realized if alteration can be mapped seismically.

B. Introduction

This report describes the development and application of models that predict the inorganic alteration that will occur (mainly in seals) when brines move in basins. The models are used to estimate the likely intensity of seal alteration. These results could be applied first to determine if the alteration is intense enough that seismic methods could provide a map of brine migration in a basin, and second to provide a theoretical basis for quantitatively interpreting such maps. This report is one in a series of reports that describe our efforts to understand physical and chemical processes in a 125 × 200 km area of the offshore Louisiana Gulf of Mexico we refer to as the GRI Corridor. The

report series is “Quantifying Gas, Oil, and Brine Migration in a 125 × 200 km Area of the Offshore Louisiana Gulf of Mexico.” The six (6) volumes that comprise this report are:

- Volume I: Executive Summary
- Volume II: Geology, Geophysics, Geochemistry and GoCAD Database
- Volume III: Organic Geochemistry
- Volume IV: Gas Washing of Oil and Its Implications
- Volume V: A Modeling Analysis of Hydrocarbon Chemistry and Gas Washing, Hydrocarbon Fluxes, and Reservoir Filling
- Volume VI: A Theoretical Analysis of the Inorganic Alteration by the Flow of Brines through Basin Seals

Now published reports from a preceding GRI project describe our concepts of capillary sealing (Cathles, 2001), laboratory investigations of capillary sealing (Shosa and Cathles, 2001), methods for interpreting the history of fluid overpressuring from porosity profiles (Revil and Cathles, 2001), geochemical models of phase fractionation (Meulbroek, 1997; Meulbroek, 1998), and implications of capillary sealing for oil production (Erendi and Cathles, 2001).

Our purpose in this report is to describe the construction of inorganic alteration models and present results of their application to hypothetical basin seals. Discussion is divided into two technical sections. The first describes the models, the second the modeling results. The most important part of the first section is the discussion of a new and simpler method of estimating the aqueous thermodynamic data.

C. Theoretical Foundations

1. Alteration Caused by Brine Flow

At temperatures above ~70°C aqueous fluids are in chemical equilibrium with the rock or sediment minerals they contact. This has been established by numerous studies over many years (Ellis, 1970; Reed and Spycher, 1984; Smith and Ehrenberg, 1989; Cathles, 1991; Cathles and Shea, 1992; Hanor, 1994). If fluids are in local chemical equilibrium with the sediment mineral they contact, their chemistry will change with temperature, pressure, and salinity. Changes in fluid chemical composition can occur only if minerals are dissolved and precipitated, that is if there is mineralogical change. This is the key to modeling mineral alteration. If the total chemical composition of a fluid can be mathematically specified as a function of a mineral buffer, temperature, pressure, and salinity, mineral alteration can be directly related to the mass of fluid moving through temperature, pressure, and salinity gradients.

Mathematically we describe the chemistry of the aqueous fluid (brine) in terms of the molar concentration of chemical basis species. The basis species are simply a minimal set of chemical species in terms of which the chemical composition of the solution can be described. The flux of basis species, i , from the fluid phase to the solid phase, J_i , in moles/cm³, is related to the amount of fluid throughput, Q' in kg/cm³, and the total concentration (i.e., the concentration of the species plus the concentration of all aqueous complexes that contain the species) of basis species i passing in and out of a unit volume of sediment, $C_{\Sigma i}$ in moles/kg fluid (Cathles and Shea, 1992):

$$J_i = Q' [C_{\Sigma i}]_{\text{in}} - Q' [C_{\Sigma i}]_{\text{out}} \quad (1)$$

Since the composition of the fluid is buffered by the specified mineral buffer, the flux of the basis species from the fluid into solid state can be inverted by multiplying it by the inverse of the transposed matrix of stoichiometric coefficients $(S_M^T)^{-1}$, to give the local mineralogic change caused by throughput Q' :

$$\Delta M_j [\text{mol/cm}^3] = (S_M^T)^{-1} J_i. \quad (2)$$

Here ΔM_j is the moles of mineral j in the buffer mineral assemblage created or destroyed in a cubic centimeter of sediment by the through-flow of Q' kg of aqueous fluid per cm^3 of sediment between the points of influx and egress. The mineral alteration can be converted to the weight fraction of the j th mineral precipitated or dissolved:

$$\Delta M_j [\text{g}_{\text{alt}} / \text{g}_{\text{sediment}}] = \frac{\Delta M_j [\text{mol/cm}^3] W_j}{\rho_{\text{sediments}}}, \quad (3)$$

where W_j is the molecular weight of buffer mineral j in gm mol^{-1} and ρ is the density of the sediments in gm cm^{-3} . $\Delta M'$ is the grams of minerals precipitated per gram of original sediment per gram of original sediment per kilogram of water flowing through a cubic centimeter of sediment.

If a gas is present in the pore fluids moving through a sedimentary basin, we must account for its effects on the chemistry of the pore fluid. The more volatile species dissolved in the liquid phase (e.g., CO_2) will separate preferentially into the gas phase and this will affect the mineralogical alteration. We can modify (1), which describes the chemical flux from the liquid to the solid buffer minerals, to accommodate fluid phases:

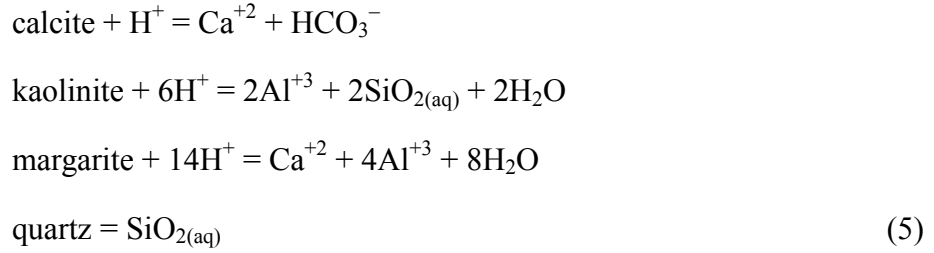
$$J_i [\text{mol/cm}^3] = Q' [\text{kg/cm}^3] \Delta_{T_2 P_2 S_2}^{T_1 P_1 S_1} (y C_{\Sigma i}^1 + [1 - y] C_{\Sigma i}^v) \quad (4)$$

where $C_{\Sigma i}^1$ is the moles of basis species i per kg of fluid in the liquid phase, $C_{\Sigma i}^v$ is the moles of basis species i per kg of solution in the vapor phase, and y is the mass fraction of total fluid flux in the liquid state at any point along the flow path, and for $\Delta_{T_2 P_2 S_2}^{T_1 P_1 S_1}$ the quantity to the right of the symbol is the difference between its value at point 1 (with temperature T_1 , pressure P_1 , and salinity S_1) and point 2 (with temperature T_2 , pressure P_2 , and salinity S_2). The liquid and vapor are assumed to be in equilibrium and the composition of the vapor is calculated from the liquid composition using Henry's Law coefficients.

Equations (2), (3), and (4) describe the alteration of a basin sediment caused by fluid flow, assuming $C_{\Sigma i}^1(T, P, S)$, and $C_{\Sigma i}^v(T, P, S)$ can be defined. The next section describes how this can be done.

2. The Buffered Chemical Composition of Basin Brines

The concentrations of the basis species in an aqueous fluid in equilibrium with a mineral buffer is specified by the dissolution reactions of the buffer minerals. Consider, for example, the chemical system spanned by the basis species Al^{+3} , Ca^{+2} , Cl^- , H_2O , HCO_3^- , H^+ , and SiO_2 . If we select calcite, kaolinite, margarite, and quartz as buffer minerals, the following chemical equations describe the dissolution of these minerals to the basis species we have chosen:



For each of these reactions, the ratio of basis species is specified by equilibrium constants, K :

$$\begin{aligned} K_{\text{calcite}} &= \frac{[\text{Ca}^{+2}][\text{HCO}_3^-]}{[\text{H}^+]} \\ K_{\text{kaolinite}} &= \frac{[\text{Al}^{+3}]^2[\text{SiO}_{2(\text{aq})}]^2}{[\text{H}^+]^6} \\ K_{\text{margarite}} &= \frac{[\text{Ca}^{+2}][\text{Al}^{+3}]^4[\text{SiO}_{2(\text{aq})}]^2}{[\text{H}^+]^{14}} \\ K_{\text{quartz}} &= [\text{SiO}_{2(\text{aq})}] \end{aligned} \quad (6)$$

If we take the logarithm of each of the mass law equations (6) we have a system of linear equations:

$$\bar{L}_{KM} = \bar{S}_M \bar{L}_{AB} \quad (7)$$

where \bar{L}_{KM} is the vector of the mineral log K , \bar{S}_M is a matrix of the stoichiometric coefficients, and \bar{L}_{AB} is the vector of log activity basis species components. For the buffer specified by (5) and (6), equation (7) is

$$\begin{bmatrix} 0 & 1 & 0 & 0 & 1 & -1 & 0 \\ 2 & 0 & 0 & 2 & 0 & -6 & 2 \\ 4 & 1 & 0 & 8 & 0 & -14 & 2 \\ 0 & 0 & 0 & 0 & 0 & 0 & 1 \end{bmatrix} \begin{bmatrix} \log a_{\text{Al}^{+3}} \\ \log a_{\text{Ca}^{+2}} \\ \log a_{\text{Cl}^-} \\ \log a_{\text{H}_2\text{O}} \\ \log a_{\text{HCO}_3^-} \\ \log a_{\text{H}^+} \\ \log a_{\text{SiO}_2} \end{bmatrix} = \begin{bmatrix} \log K_{\text{calcite}} \\ \log K_{\text{kaolinite}} \\ \log K_{\text{margarite}} \\ \log K_{\text{quartz}} \end{bmatrix} \quad (8)$$

Note we have reversed the order of (7). Equation (8) cannot be solved because it contains seven unknowns (the activities of the basis species a_i) and there are only four mass action equations. However, we can remove three of the unknowns from the system by independently specifying the salinity (m_{Cl^-}), which is rarely mineralogically buffered, solving for the pH using charge balance (see later discussion), and assuming that $a_{\text{H}_2\text{O}} = 1$. Mathematically we write

$$\bar{L}_{KM} = \bar{\bar{S}}'_M \bar{L}_{AB} + \bar{S}_M^{\text{Cl}^-} \log a_{\text{Cl}^-} + \bar{S}_M^{\text{H}^+} \log a_{\text{H}^+} + \bar{S}_M^{\text{H}_2\text{O}} \log a_{\text{H}_2\text{O}}, \quad (9)$$

where $\bar{\bar{S}}'_M$ is the stoichiometric reduced by removing the Cl^- , H_2O , and H^+ columns, and $\bar{S}_M^{\text{Cl}^-}$, $\bar{S}_M^{\text{H}^+}$, and $\bar{S}_M^{\text{H}_2\text{O}}$ are the column vectors removed. Since none of the minerals contain Cl^- , $\bar{S}_M^{\text{Cl}^-}$ contains all zeros and this term can be dropped. The $\log a_{\text{H}_2\text{O}}$ is zero if we assume, as we shall do, that $a_{\text{H}_2\text{O}} = 1$. Taking these changes and multiplying both sides of (9) with the inverse of the reduced stoichiometric matrix, (9) becomes:

$$\bar{L}_{AB} = \bar{\bar{S}}'^{-1}_M \left[\bar{L}_{KM} + \left(\log a_{\text{H}^+} \right) \bar{S}_M^{\text{H}^+} \right], \quad (10)$$

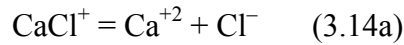
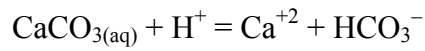
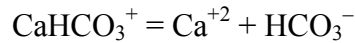
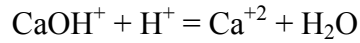
where $\bar{\bar{S}}'^{-1}_M$ is the inverse of the reduced stoichiometric matrix. For the mineral buffer we have chosen as an example, (10) becomes:

$$\begin{bmatrix} \log \left(\frac{a_{\text{Al}^{+3}}}{(a_{\text{H}^+})^3} \right) \\ \log \left(\frac{a_{\text{Ca}^{+2}}}{(a_{\text{H}^+})^2} \right) \\ \log a_{\text{HCO}_3^-} a_{\text{H}^+} \\ \log a_{\text{SiO}_2} \end{bmatrix} = \begin{bmatrix} 0 & 0 & 1 & 0 \\ 0.5 & -2 & 2 & 0 \\ 0 & 1 & -1 & 0 \\ -1 & 2 & -2 & 1 \end{bmatrix} \begin{bmatrix} \log K_{\text{calcite}} \\ \log K_{\text{kaolinite}} \\ \log K_{\text{margarite}} \\ \log K_{\text{quartz}} \end{bmatrix} \quad (11)$$

In other words, the log activity ratios of the basis species are determined by the dissolution log K of the mineral buffer.

The activities calculated in this way are the activities of the individual basis species. For the transport equation we need the total concentration (not activity) of all aqueous complexes that contain each basis species. For example, Ca^{+2} will commonly complex to varying degrees with OH^- , HCO_3^- , CO_3^{-2} , and Cl^- . This complexation must be taken into account to specify the total concentration of Ca^{+2} in solution.

The log activity of aqueous complexes can be calculated from the activities of the basis species, the stoichiometry of the aqueous complexes, and the dissociation constants of the complexes. Consider, for example, the complexes CaOH^+ , CaHCO_3^+ , $\text{CaCO}_{3(\text{aq})}$, CaCl^+ , CaCl_2 . Dissociation of these complexes to the basis species we have chosen can be written:



The mass action equations for these reactions are

$$K_{\text{CaOH}^+} = \frac{(\text{Ca}^{+2})}{(\text{H}^+)(\text{CaOH}^+)}$$

$$K_{\text{CaCO}_3} = \frac{(\text{Ca}^{+2})(\text{HCO}_3^-)}{(\text{H}^+)(\text{CaCO}_{3(\text{aq})})}$$

$$K_{\text{CaHCO}_3^+} = \frac{(\text{Ca}^{+2})(\text{HCO}_3^-)}{(\text{CaHCO}_3^+)}$$

$$K_{\text{CaCl}^+} = \frac{(\text{Ca}^{+2})(\text{Cl}^-)}{(\text{CaCl}^+)}$$

$$K_{\text{CaCl}_2} = \frac{(\text{Ca}^{+2})(\text{Cl}^-)^2}{(\text{CaCl}_2)} \quad (13)$$

Taking the log of (13) as we did for (6) we obtain an equation similar to (7):

$$\bar{L}_{AS} = \bar{S}_S \bar{L}_{AB} - \bar{L}_{KS}, \quad (14)$$

where \bar{L}_{AS} are the log activities of the aqueous complexes, \bar{S}_S is the matrix of the stoichiometric coefficients in (12), and \bar{L}_{AB} are the log activities of the basis species, and \bar{L}_{KS} are the log of the dissociation constants of the aqueous complexes. For the complexes in (12), (14) can be written:

$$\begin{bmatrix} \log a_{\text{CaOH}^+} \\ \log a_{\text{CaHCO}_3^+} \\ \log a_{\text{CaCO}_3(\text{aq})} \\ \log a_{\text{CaCl}^+} \\ \log a_{\text{CaCl}_2} \end{bmatrix} = \begin{bmatrix} 1 & 0 & 1 & 0 & -1 \\ 1 & 0 & 0 & 1 & 0 \\ 1 & 0 & 0 & 1 & -1 \\ 1 & 1 & 0 & 0 & 0 \\ 1 & 2 & 0 & 0 & 0 \end{bmatrix} \begin{bmatrix} \log a_{\text{Ca}^{+2}} \\ \log a_{\text{Cl}^-} \\ \log a_{\text{H}_2\text{O}} \\ \log a_{\text{HCO}_3^-} \\ \log a_{\text{H}^+} \end{bmatrix} - \begin{bmatrix} \log K_{\text{CaOH}^+} \\ \log K_{\text{CaHCO}_3^+} \\ \log K_{\text{CaCO}_3(\text{aq})} \\ \log K_{\text{CaCl}^+} \\ \log K_{\text{CaCl}_2} \end{bmatrix} \quad (15)$$

If the pH, the activities of the basis species, and the $\log K$ of the dissociation reactions are known, the activities of the aqueous complexes are specified by (15).

To obtain the activity of the basis species we determine a_{H^+} by charge balance. For the above example charge balance requires:

$$3m_{\text{Al}^{+3}} + 2m_{\text{Ca}^{+2}} + m_{\text{H}^+} + m_{\text{CaOH}^+} + m_{\text{CaHCO}_3^+} + m_{\text{CaCl}^+} = m_{\text{Cl}^-} + m_{\text{HCO}_3^-} \quad (16)$$

where m_i is the concentration of the basis species or complexes. To solve, we rewrite (16) in terms of the activities of the aqueous ions (except for the chloride ion concentration that is specified independently):

$$3 \frac{a_{\text{Al}^{+3}}}{\gamma_{\text{Al}^{+3}}} + 2 \frac{a_{\text{Ca}^{+2}}}{\gamma_{\text{Ca}^{+2}}} + a_{\text{H}^+} + \frac{a_{\text{CaOH}^+}}{\gamma_{\text{CaOH}^+}} + \frac{a_{\text{CaHCO}_3^+}}{\gamma_{\text{CaHCO}_3^+}} + \frac{a_{\text{CaCl}^+}}{\gamma_{\text{CaCl}^+}} = m_{\text{Cl}^-} + \frac{a_{\text{HCO}_3^-}}{\gamma_{\text{HCO}_3^-}} \quad (17)$$

Here a_i are the activities of the basis species and γ_i are the activity coefficients of the basis species. The activity coefficients are calculated using the Debye-Huckel equation (Stumm and Morgan, 1980):

$$-\log \gamma_i = \frac{A(T)Z_i^2 I^{1/2}}{1 + a B(T) I^{1/2}} \quad (18)$$

where $A(T)$ and $B(T)$ are functions of the dielectric constant of water:

$$A(T) = 1.82 \times 10^6 (\epsilon T)^{-3/2} \quad (19)$$

$$B(T) = 50.3(\epsilon T)^{-1/2} \quad (20)$$

Z_i is the charge of the ion, I is the ionic strength of the solution ($I = 0.5 \sum C_i Z_i^2$) and a^o is a parameter that describes the size of the ion. We can rewrite the charge balance equation (17) as a polynomial in a_{H^+} using (11) and (15):

$$\begin{aligned} & 3 \frac{C_{Al^{+3}}}{\gamma_{Al^{+3}}} (a_{H^+})^3 + \left(2 \frac{C_{Ca^{+2}}}{\gamma_{Ca^{+2}}} + \frac{C_{Ca^{+2}} C_{Cl^-}}{K_{CaCl^+}} \right) (a_{H^+})^2 \\ & + \left(1 + \frac{C_{Ca^{+2}} C_{Cl^-}}{K_{CaOH^+}} + \frac{C_{Ca^{+2}} C_{HCO_3^-}}{K_{CaHCO_3^-}} \right) a_{H^+} - m_{Cl^-} - C_{HCO_3^-} (a_{H^+})^{-1} = 0 \end{aligned} \quad (21)$$

This equation can be solved iteratively for its one positive root.

Thus the total chemistry of an aqueous fluid can be calculated if the log K dissolution constants of a set of buffer minerals and the log K of the dissociation reactions of all significant aqueous complexes are known. The issues, and it is a big one, is now to specify these log K values for temperatures, pressures, and salinities of interest. If this can be done, the alteration of seals in basins by the forced through-flow of brine can be calculated.

3. Calculating Dissolution and Dissociation Log K

To calculate solution composition from a mineral buffer we need dissolution and dissociation log K at the appropriate temperatures and pressures. Few of these have been directly measured and so it is common practice to estimate them from other, more available thermodynamic data. We first show how this has been done and then suggest how it can be done better for aqueous species.

The log K_{PT} values for minerals, gases, and aqueous species are related to the standard partial molar Gibbs free energy ($\Delta \bar{G}_{PT}^o$):

$$\log K_{PT} = \frac{-\Delta \bar{G}_{PT}^o}{2.303RT}, \quad (22)$$

where R is the gas constant (1.987×10^{-3} kcal deg $^{-1}$ mol $^{-1}$) and T is temperature in K. The partial molar Gibbs free energy of a species is a perfect differential that can be expanded:

$$d\Delta \bar{G}_{PT}^o = \bar{V}^o dP - \bar{S}^o dT \quad (23)$$

where \bar{V}^o is the standard partial molar volume and \bar{S}^o is the standard partial molar entropy. By definition:

$$\bar{V}^o = \left(\frac{\partial \Delta \bar{G}_{PT}^o}{\partial P} \right)_T \quad (24)$$

$$\bar{S}^o = \left(\frac{\partial \Delta \bar{G}_{PT}^o}{\partial T} \right)_P \quad (25)$$

Integration of (23) from a standard state at which $\Delta \bar{G}_{PT}^o = \Delta \bar{G}_{25^\circ\text{C}, 1\text{bar}}^o$ yields:

$$\Delta \bar{G}_{PT}^o = \Delta \bar{G}_{25^\circ\text{C}, 1\text{bar}}^o - \int_{298.15}^T \bar{S}^o dT + \int_1^P \bar{V}^o dP \quad (26)$$

In the next section, we will first derive equations of state from (26) that are appropriate for minerals and gases, and then an equation of state suitable for aqueous species. After each equation is developed, we discuss procedures for estimating the equation parameters.

a. Equations of State for Minerals and Gases

By the definition of the standard partial molar heat capacity ($\Delta \bar{C}_P^o$):

$$d\bar{S}^o = \frac{\Delta \bar{C}_P^o dT}{T}, \quad (27)$$

and thus:

$$\bar{S}_{PT}^o = \bar{S}_{25^\circ\text{C}, 1\text{bar}}^o + \int_{298.15}^T \frac{\Delta \bar{C}_P^o}{T} dT \quad (28)$$

This equation can be integrated analytically if $\Delta \bar{C}_P^o(T)$ can be expressed as a polynomial function of temperature. Many power series expansions have been proposed (e.g., Robinson and Haas, 1983; Fei and Saxena, 1987), but the most commonly used is still the one originally suggested by Maier and Kelly (1932):

$$\Delta \bar{C}_P^o = a + bT - \frac{c}{T^2}. \quad (29)$$

Defining $T_{\text{ref}} = 298.15$ K and substituting into (26) yields:

$$\int_{T_{\text{ref}}}^T \bar{S}_{PT}^o dT = \bar{S}_{\text{ref}}^o (T - T_{\text{ref}}) + a \ln(T - T_{\text{ref}}) + b(T - T_{\text{ref}}) + \frac{c}{2} \left(\frac{1}{T^2} - \frac{1}{T_{\text{ref}}^2} \right). \quad (30)$$

The pressure integral in (26) is usually evaluated assuming that the decrease in volume due to compression and the increase in volume due to thermal expansion cancel, and that, therefore \bar{V}^o is a constant. This appears to be a valid assumption within the overall uncertainty in the Gibbs free energy (Nordstrom and Munoz, 1985).

For constant \bar{V}^o :

$$\int_1^P \bar{V}^o dP = \bar{V}_{25^\circ\text{C}, 1\text{bar}}^o \int_1^P dP = \bar{V}_{25^\circ\text{C}, 1\text{bar}}^o (P - 1). \quad (31)$$

Equations (30) and (31) complete the equation of state (26), allowing the standard Gibbs free energy at P and T to be calculated from that at 25°C and 1 bar using 4 parameters: a , b , c , and $\bar{V}_{25^\circ\text{C}, 1\text{bar}}^o$.

b. Estimating Gibbs Free Energies of Silicate Minerals

The thermodynamic data for silicate minerals is essential to the calculation of geochemical equilibria in sedimentary basins. There are a number of reasonably comprehensive, internally consistent databases that provide thermodynamic data for many of the common minerals (e.g., Robie and Hemingway, 1995). However, there are minerals in sedimentary basins that are compositionally variable (e.g., chlorites and clay minerals) for which measured Gibbs free energies do not exist.

The stoichiometric complexities of silicate minerals arise in mainly three crystallographic sites: (1) Al^{+3} substitutes for Si^{+4} in the tetrahedral sites, (2) the octahedral sites house a variety of +2 and +3 cations (e.g., Mg^{+2} , Fe^{+2} , Fe^{+3}) and, (3) large, ionically-bound cations (Na^+ , K^+ , Mg^+ , and Ca^{+2}) which occupy sites between the tetrahedral and octahedral layers to maintain charge balance in a mineral structure disturbed by Al-substitution or different charges on the octahedral cations.

Structurally, silicate materials can be constructed by combining a number of polyhedral components (tetrahedra and octahedra) and this fact provides the basis for many of the empirical relationships between mineral structure and the physical properties of minerals (including thermochemical data) (Hazen, 1988). The phyllosilicate minerals (e.g., the clay minerals and chlorites) are composed of sheets of SiO_4 tetrahedra and $\text{X}(\text{OH})_6$ octahedra, where X is generally Mg^{+2} , Fe^{+2} , Fe^{+3} , or Al^{+3} . Clay minerals (e.g., illites) may require interlayer cations to meet charge balance conditions.

Chermak and Rimstidt (1989) have determined by multiple regression of the Gibbs free energies of a number of silicate minerals, the polyhedral contributions (g_i) of oxide and hydroxide components to the total Gibbs free energies of a selected group of silicate minerals. Using these polyhedral components, the ΔG_f^o of silicate minerals at 25°C and 1 bar can be estimated from the stoichiometrically-weighted sum of the contributions of each oxide or hydroxide component:

$$\Delta G_f^o = \sum_{f=1}^n \nu_i g_i \quad (32)$$

where ν_i is the number of moles of oxide or hydroxide components per formula unit. The Gibbs free energy of formation for oxide/hydroxide polyhedral components is related to g_i :

$$g_i = -9.397 + 0.994 (\Delta G_{\text{oxide/hydroxide}}). \quad (33)$$

Examples of the use of Chermak and Rimstidt's methods can be found in Shosa (2000).

c. Equations of State for Aqueous Species

Equation (26) applies for aqueous species as well, but deriving integrable expressions for the entropy and volume changes with temperature and pressure is a little more complicated. The most commonly used form of the equation of state (26) is the revised-HKF equation of state (Helgeson and Kirkham, 1976; Tanger and Helgeson, 1988):

$$\begin{aligned} \Delta \bar{G}_{PT}^o &= \Delta \bar{G}_{\text{ref}}^o - S_{\text{ref}}(T - T_{\text{ref}}) + a_1(P - P_{\text{ref}}) \\ &+ a_2 \ln\left(\frac{\Psi + P}{\Psi + P_{\text{ref}}}\right) + \left(\frac{1}{T - \Theta}\right) \left[a_3(P - P_{\text{ref}}) + a_4 \ln\left(\frac{\Psi + P}{\Psi + P_{\text{ref}}}\right) \right] \\ &- c_1 \left[T \ln\left(\frac{T}{T_{\text{ref}}}\right) - T + T_{\text{ref}} \right] \\ &- c_2 \left\{ \left[\left(\frac{1}{T - \Theta}\right) - \frac{1}{T_{\text{ref}} - \Theta} \right] \left(\frac{\Theta - T}{\Theta} \right) - \frac{T}{\Theta^2} \ln \left[\frac{T_{\text{ref}}(T - \Theta)}{T(T_{\text{ref}} - \Theta)} \right] \right\} \\ &+ \omega \left(\frac{1}{\mathcal{E}_{PT}} - 1 \right) - \omega_{\text{ref}} \left(\frac{1}{\mathcal{E}_{\text{ref}}} - 1 \right) + \omega_{\text{ref}} Y_{\text{ref}}(T - T_{\text{ref}}) \end{aligned} \quad (34)$$

A full discussion of the derivation of this equation of state can be found in Tanger and Helgeson (1988) and Helgeson and Kirkham (1976). Here we give only a brief commentary on how (34) is obtained from (26).

The standard partial molal volume (\bar{V}^o) of an aqueous ion can be expressed as the sum of the intrinsic volume of the ion (\bar{V}_I^o), the change in volume due to local collapse of the solvent ($\Delta \bar{V}_e^o$), and the change in volume due to the solvation of the ion ($\Delta \bar{V}_s^o$) (Helgeson and Kirkham, 1976):

$$\bar{V}^o = \bar{V}_I^o + \Delta \bar{V}_e^o + \Delta \bar{V}_s^o. \quad (35)$$

The “non-solvation” contribution to the volume of an aqueous species can be described as a function of temperature:

$$\Delta\bar{V}_n^o = \bar{V}_I^o + \Delta\bar{V}_e^o = \sigma + \xi \left(\frac{1}{T - \Theta} \right), \quad (36)$$

where σ and ξ are species-dependent, pressure-dependent, temperature-independent coefficients, and Θ represents a solvent parameter which for water equals 228 K. The pressure dependencies of σ and ξ are expressed:

$$\sigma = a_1 + a_2 \left(\frac{1}{\Psi + P} \right), \quad (37)$$

$$\xi = a_3 + a_4 \left(\frac{1}{\Psi + P} \right), \quad (38)$$

where a_1 , a_2 , a_3 , and a_4 are species-dependent, temperature- and pressure-independent coefficients, and Ψ represents another solvent parameter which for water equals 2800 bars (Tanger and Helgeson, 1988). The non-solvation contribution to the volume of an aqueous species is thus:

$$\Delta\bar{V}_n^o = a_1 + a_2 \left(\frac{1}{\Psi + P} \right) + \left(\frac{1}{T - \theta} \right) \left[a_3 + a_4 \left(\frac{1}{\Psi + P} \right) \right] \quad (39)$$

The change in Gibbs free energy due to solvation effects is given by the Born equation (Born, 1920):

$$\Delta\bar{G}_s^o = \omega \left(\frac{1}{\varepsilon} - 1 \right), \quad (40)$$

where ε is the dielectric constant of the solvent and ω is the Born coefficient,

$$\omega = \frac{N_a (Z_i e)^2}{2r_{e,i}} \quad (41)$$

N_a is Avogadro's number ($6.02252 \times 10^{23} \text{ mol}^{-1}$), Z_i is the charge of species, e is the absolute electronic charge ($4.80298 \times 10^{-10} \text{ esu}$), $r_{e,i}$ is the effective radius of species.

The change in volume due to solvation effects is obtained by taking the derivative of (40) with respect to pressure at constant temperature:

$$\Delta\bar{V}_s^o = \left(\frac{\partial \Delta\bar{G}_s^o}{\partial P} \right)_T = -\omega Q + \left(\frac{1}{\varepsilon} - 1 \right) \left(\frac{\partial \omega}{\partial P} \right)_T, \quad (42)$$

where Q is defined:

$$Q \equiv \frac{1}{\varepsilon} \left(\frac{\partial \ln \varepsilon}{\partial P} \right)_T \quad (43)$$

Substituting yields:

$$\Delta \bar{V}^o = a_1 + a_2 \left(\frac{1}{\Psi + P} \right) + \left[a_3 + a_4 \left(\frac{1}{\Psi + P} \right) \right] \left[\frac{1}{T - \Theta} \right] - \omega Q + \left(\frac{1}{\varepsilon} - 1 \right) \left(\frac{\partial \omega}{\partial P} \right)_T. \quad (44)$$

This equation can be substituted into (26) and integrated to give the change in Gibbs free energy due to changes in pressure.

The entropy integral in (26) can be expressed in terms of heat capacity as shown in (28). The standard partial molal heat capacity, ΔC_P^o , can be expanded in a fashion similar to (35):

$$\Delta \bar{C}_P^o = \bar{C}_{P,1}^o + \Delta \bar{C}_{P,e}^o + \Delta \bar{C}_{P,s}^o \quad (45)$$

The temperature dependence of the non-solvation contributions can be represented

$$\Delta \bar{C}_{P,n}^o = \bar{C}_{P,1}^o + \Delta \bar{C}_{P,e}^o = c_1 + c_2 \left(\frac{1}{T - \Theta} \right)^2, \quad (46)$$

where c_1 and c_2 depend only on the aqueous species (e.g., do not depend on temperature and pressure). Using the thermodynamic identity

$$\left(\frac{\partial^2 \bar{V}_n^o}{\partial T^2} \right) = -\frac{1}{T} \left(\frac{\partial \bar{C}_{P,n}^o}{\partial P} \right)_T, \quad (47)$$

the heat capacity obtained by differentiating (44) twice is:

$$\Delta \bar{C}_{P,n}^o = c_1 + c_2 \left(\frac{1}{T - \Theta} \right)^2 - 2T \left(\frac{1}{T - \Theta} \right)^3 \left(a_3 (P - P_r) + a_4 \left(\frac{\Psi + P}{\Psi + P_r} \right) \right). \quad (48)$$

The solvation contribution to the change in heat capacity is obtained by differentiating the Born equation twice with respect to temperature:

$$\Delta C_{P,s}^o = \omega TX + 2TY \left(\frac{\partial \omega}{\partial T} \right)_P - T \left(\frac{1}{\varepsilon} - 1 \right) \left(\frac{\partial^2 \omega}{\partial T^2} \right)_P, \quad (49)$$

where X and Y are also Born functions:

$$X \equiv \frac{1}{\varepsilon} \left[\left(\frac{\partial^2 \varepsilon}{\partial T^2} \right)_P - \left(\frac{\partial \ln \varepsilon}{\partial T} \right)_P^2 \right] \quad (50)$$

$$Y \equiv \frac{1}{\varepsilon} \left(\frac{\partial \ln \varepsilon}{\partial T} \right)_P \quad (51)$$

Substituting (48) and (49) into (45) yields the equation of state for the standard partial molal heat capacity of an ion or electrolyte as a function of pressure and temperature (Tanger and Helgeson, 1988):

$$\begin{aligned} \Delta \bar{C}_{P,n}^o = & c_1 + c_2 \left(\frac{1}{T - \Theta} \right)^2 - 2T \left(\frac{1}{T - \Theta} \right)^3 \left[a_3(P - P_r) + a_4 \left(\frac{\Psi + P}{\Psi + P_r} \right) \right] \\ & + \omega TX + 2TY \left(\frac{\partial \omega}{\partial T} \right)_P - T \left(\frac{1}{\varepsilon} - 1 \right) \left(\frac{\partial^2 \omega}{\partial T^2} \right)_P \end{aligned} \quad (52)$$

Integration of (52) with respect to temperature in (26) gives the equation of state for changes in standard partial molal entropy from the standard state:

$$\begin{aligned} \Delta S_{PT}^o - \Delta S_{25^\circ\text{C}, 1\text{bar}}^o = & c_1 \ln \left(\frac{T}{T_{\text{ref}}} \right) - \frac{c_2}{\Theta} \left[\left(\frac{1}{T - \Theta} \right) - \left(\frac{1}{T_{\text{ref}} - \Theta} \right) \right] + \frac{1}{\Theta} \ln \left(\frac{T_{\text{ref}}(T - \Theta)}{T(T_{\text{ref}} - \Theta)} \right) \\ & + \left(\frac{1}{T - \Theta} \right)^2 \left[a_3(P - P_{\text{ref}}) + a_4 \ln \left(\frac{\Psi + P}{\Psi + P_{\text{ref}}} \right) \right] \\ & + \omega Y - \left(\frac{1}{\varepsilon} - 1 \right) \left(\frac{\partial \omega}{\partial T} \right)_P - \omega_{\text{ref}} Y_{\text{ref}} \end{aligned} \quad (53)$$

In this equation ref refers to standard conditions of $P = 1$ bar and $T = 25^\circ\text{C}$.

Substitution of (44) and (53) into (26) yields the HKF equation of state, equation (34). Our discussion shows that fundamentally the HKF equation of state simply accounts for the effects of change in solvation on heat capacity.

d. Parameters for the HKF Equation of State

There are a number of coefficients and parameters in (34) that must be defined before we can solve for the Gibbs free energy of a species at elevated temperature and pressure. We need to know: (1) the dielectric constant of water as a function of temperature and pressure, (2) the Gibbs free energy of water as a function of temperature and pressure, (3) the standard partial molar Gibbs free energies (ΔG_f^o) and entropies (\bar{S}^o) at 25°C and 1 bar for any species of interest including water (tabulated), (4) the equation of state coefficients for minerals (i.e., the Maier-Kelly coefficients, tabulated), and (5) the seven equation of state coefficients for the revised-HKF equation of state for aqueous species (a_1 to a_4 , c_1 , c_2 , and ω).

1. The dielectric constant of water

We use a fourth degree power function of temperature and density defined empirically by Helgeson and Kirkham (1974) to calculate the dielectric constant of water (ϵ) as a function of temperature and pressure:

$$\epsilon = \sum_{i=0}^4 \sum_{j=0}^{4-i} e_{ij} T^i \rho^j \quad (54)$$

The regression coefficients e_{ij} are given in Helgeson and Kirkham (1974) and Shosa (2000); ρ is the density of water.

2. The Gibbs free energy of water

The Gibbs free energy of water was not calculated at each temperature and pressure in our calculations. Instead, the values for the Gibbs free energy of water at the temperature and pressure of interest were obtained by interpolating between “smoothed values” in Table 29 of Helgeson and Kirkham (1974) using a bicubic interpolation.

We smoothed the table because derivatives of the surface defined by the table, ($\Delta G_{\text{H}_2\text{O}} = f(T, P)$), oscillated (Figure 1a) and produced mineralogical alteration that we did not think were real.

The smoothing of Helgeson and Kirkham’s Gibbs free energy of water table was accomplished by fitting polynomials of the form:

$$\Delta G_{\text{H}_2\text{O}}(T) = \sum_{k=1}^2 a_k(T) P^k \quad (55)$$

for each temperature listed in the table. This procedure yields four coefficients for each of the temperatures. A polynomial of the form:

$$a_k(T) = \sum_{l=-1}^4 c_{l,k} T^l \quad (56)$$

was then fit to the coefficients for each value of pressure listed in the table. A new table of Gibbs free energies is then generated using

$$\Delta G_{\text{H}_2\text{O}}(P, T) = \sum_{k=-1}^2 \left(\sum_{l=-1}^4 c_{l,k} T^l \right) P^k. \quad (57)$$

Bicubic interpolation is used to interpolate between these “smoothed” table values. The maximum change in any table entry was a few percent of the original Gibbs free energy values, but the procedure removed the variations in the Gibbs free energy of water as shown in Figure 1b, at least below 2 km, the depths of interest in this study.

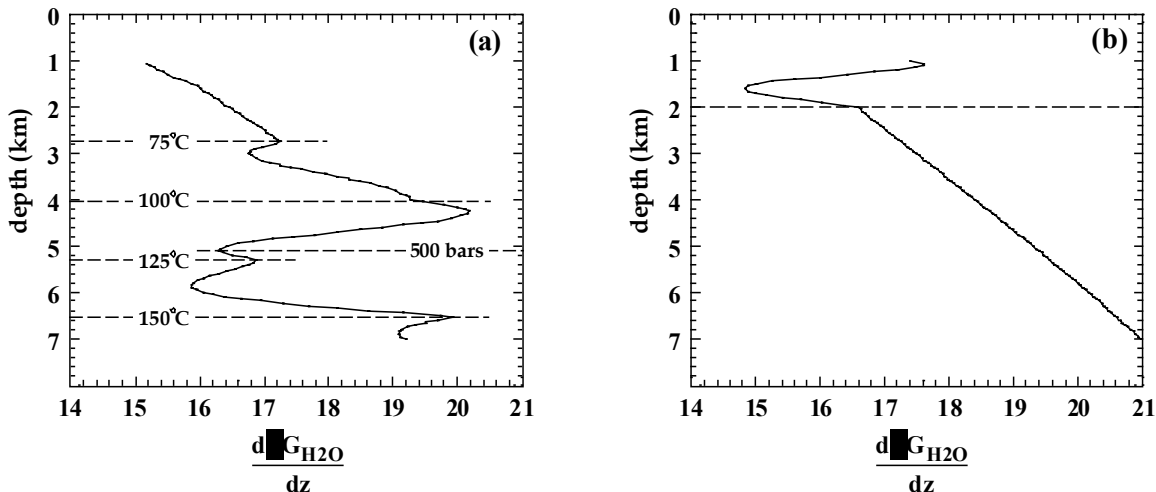


Figure 1: The derivative the Gibbs free energy of water as a function of depth. (A) Gibbs free energy interpolated from Table 29 in Helgeson and Kirkham (1974). (B) Gibbs free energy interpolated from transformed and smoothed table.

3. Estimating the revised-HKF equation of state coefficients

The revised-HKF equation of state requires seven species-dependent regression coefficients (ω , a_1 , a_2 , a_3 , a_4 , c_1 , and c_2).

All seven coefficients are important. This can be illustrated by calculating the Gibbs free energies for all of the 685 aqueous species for which published coefficients exist and creating histograms of the error in $\log K$, where the error is defined as the difference between the $\log K$ calculated using the coefficients and the $\log K$ calculated assuming the coefficients are zero. At 50°C, the $\log K$ values are all within ± 0.5 log units (an assumed “acceptable” error based on the experimental error in measured Gibbs free energies [Helgeson, 1974]). At 100°C and 1 bar, 5% of the species have an error in $\log K$ of greater than 0.5 log units, at 150°C and 4.86 bar this percentage increases to 28%. At 300°C and 85.93 bar, less than one-third of the $\log K$ values are within acceptable error limits. The percentage of aqueous species with errors in calculated $\log K$ increases with temperature and pressure.

Unfortunately, experimentally measured volumes and heat capacities at elevated temperatures and pressures are not available for many aqueous ions and electrolytes. A number of empirical algorithms have been developed that allow the estimation of the coefficients of the revised-HKF equation of state. The published procedures are involved and are summarized in Shock and Helgeson (1988; table 8), Shock et al. (1997), and p. 93-96 of Shosa (2000).

D. Simplified Estimation of the Revised-HKF Equation of State Coefficients

The simplification of the empirical relationships between thermodynamic parameters and equation of state coefficients results from the fact that, without *any* loss of accuracy, (1) the Born coefficient, ω , can be expressed as a simple function of standard state entropy and charge, (2) the volume coefficients a_2 , a_3 , and a_4 can be expressed as linear

functions of a_1 , (3) the heat capacity coefficient c_2 can be expressed as a linear function of c_1 and charge, and (4) both a_1 and c_1 can be linearly related to standard state entropy. In other words the seven parameters of the HKF equation of state (a_1 - a_4 , c_1 - c_2 , and ω) can be reduced to three parameters, a_1 , c_1 , and ω . Further, a_1 , c_1 , and ω are linear functions of standard state entropy.

1. The Born Coefficient as a Function of Standard State Entropy and Charge

Figure 2a plots published ω values of species for which both experimentally determined and estimated data exist (Johnson et al., 1992; Shock and Helgeson, 1988; Shock et al., 1997; Sverjensky et al., 1997) as a function of the standard state entropy and charge of the species. The following equation can be obtained by linear regression:

$$\omega = 0.05 + (0.5|Z|)\xi_{\pm} - (0.015S_i). \quad (58)$$

where $\xi_+ = 1$, $\xi_- = 3$, and the subscript + indicates a positively charged species, and subscript - indicates a negatively charged species. Uncharged species (other than the noble and diatomic gases) have negligible solvation effects so $\omega = 0$. The Born coefficient for noble and diatomic gases is given by:

$$\omega = -(0.015S_i). \quad (59)$$

Born coefficients estimated using (58) are plotted against published values in Figure 3. The slope of the line is 0.998 and the intercept so close to zero (-0.015) that (58) clearly provides as good an estimate of ω as the literature values. Furthermore, there is no systematic relationship between the aqueous species whose Born coefficients are not predicted well by (58). Chloride species (AuCl_4^-) as well as oxide species (MnO_2^-) are found in this subset and positively charged species (UO_2^+) fall into this group as well. If we calculate Gibbs free energies of the off-regression species along the saturation curve using both published-HKF equation of state parameters and those we predict from our regressions (including those that will be presented below), we find that the predicted log K values diverge only near the critical point of water (374°C).

2. Reduction of a_i to a_1

Figure 4 plots volume equation of state coefficients (a_2 , a_3 , and a_4) for the 685 dissolved aqueous species for which published data exist as a function of a_1 . The following equations can be deduced by linear regression:

$$\begin{aligned} a_2 &= -752 + 2400 a_1 \\ a_3 &= 8.57 - 9.30 a_1 \\ a_4 &= -24700 - 9970 a_1 \end{aligned} \quad (60)$$

These relationships apply even for those species that do not lie directly on the regression line. If we calculate the change in volume due to non-solvation contributions for these species using (39), the published and calculated $\Delta \bar{V}_n$ agree (see Figure 5).

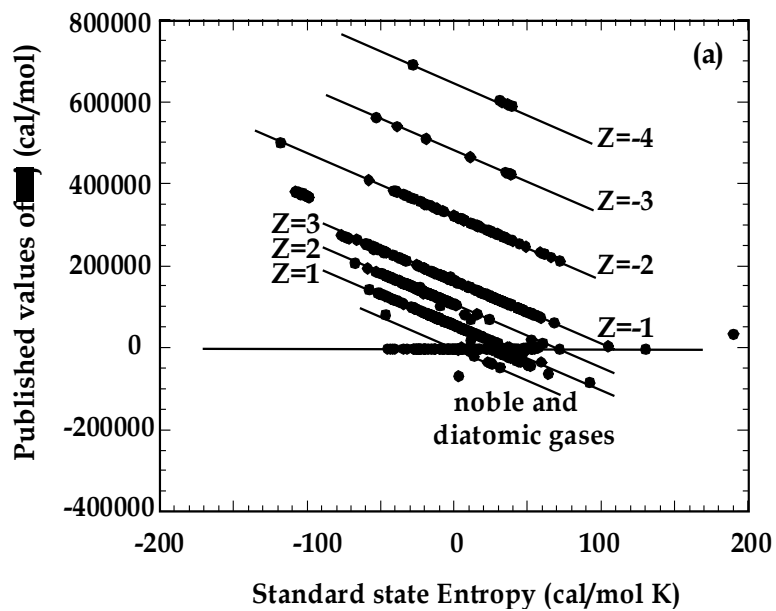


Figure 2a: Published values of the Born coefficient, ω (Johnson et al., 1991; Shock and Helgeson, 1988; Shock et al., 1997; Sverjensky et al., 1997) as a function of the partial molal standard state entropy, S° .

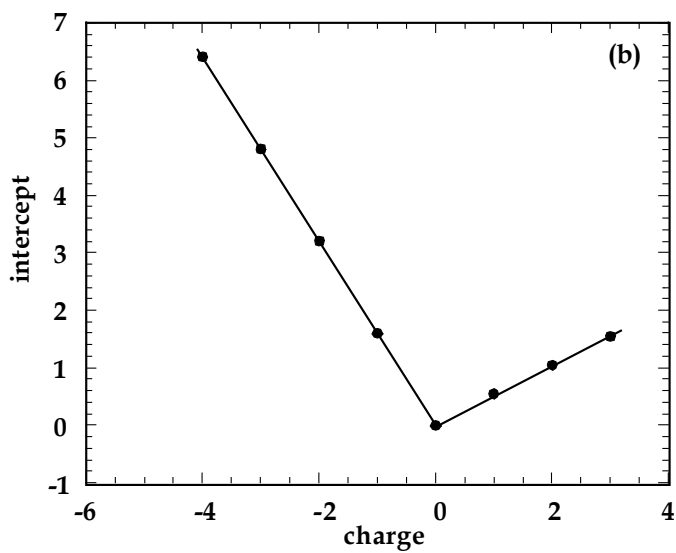


Figure 2b: Intercepts of the regression lines through the data in (2a) as a function of charge.

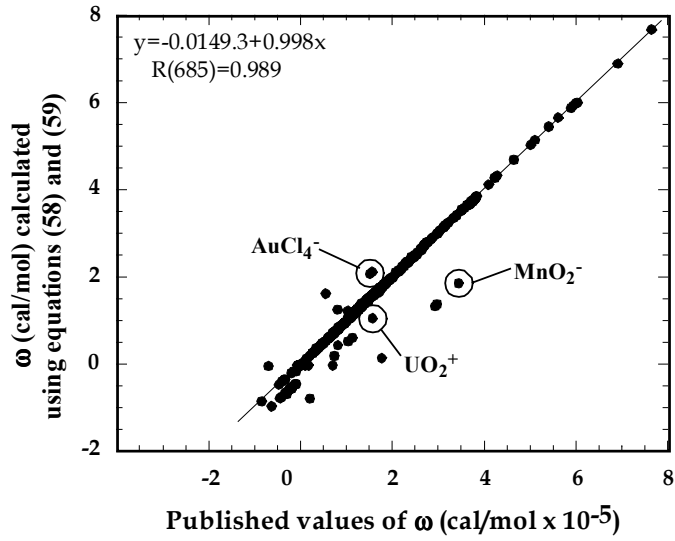


Figure 3: The Born coefficient, ω , calculated using equations (58) and (59) as functions of published values of ω (Johnson et al., 1991; Shock and Helgeson, 1988; Shock et al., 1997; Sverjensky et al., 1997).

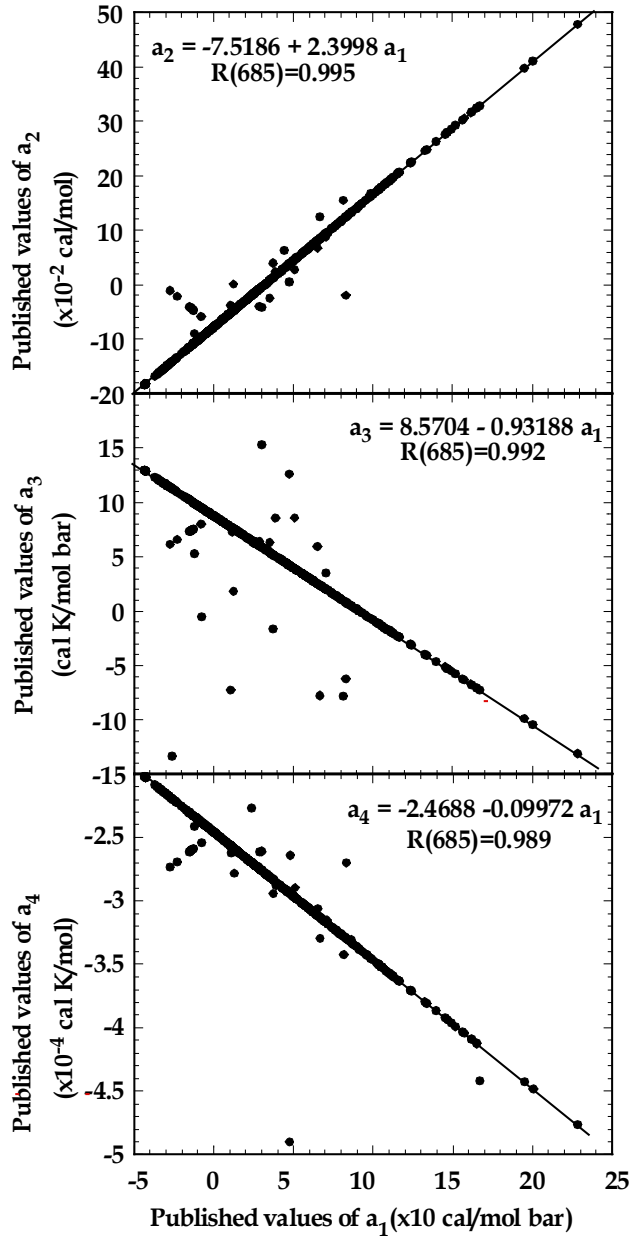


Figure 4: The published values of the revised-HKF equation of state volume coefficients (a_2 , a_3 , and a_4) as a function of a_1 .

3. Reduction of c_i to c_1

If we separate the aqueous species by charge, c_2 is clearly a linear function of c_1 . This is shown in Figures 5-7. The regression equation fitting all data is

$$c_2 = \begin{cases} -2.05c_1, & \text{if } Z \geq 0 \\ 4.65c_1, & \text{if } Z < 0 \end{cases} - 5.34. \quad (61)$$

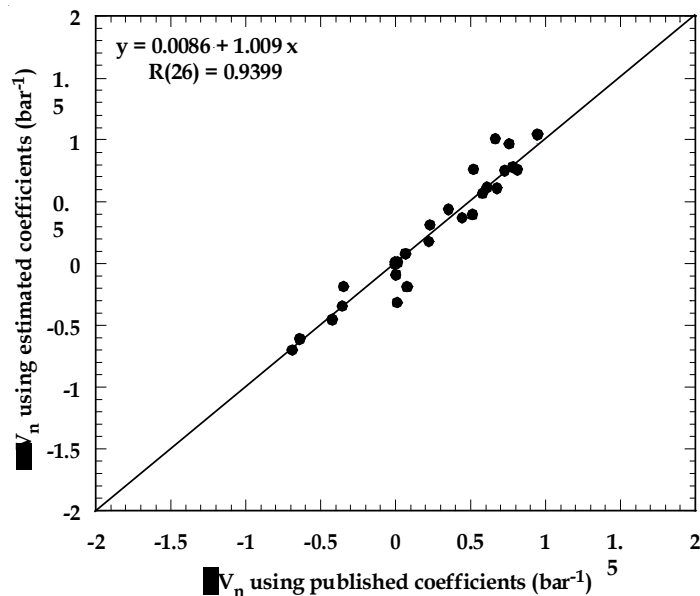


Figure 5: Comparison of the non-solvation contribution to volume (ΔV_n) calculated from (37) using published values of a_1 , and a_2 , a_3 , and a_4 and a_1 and equation (60). Only the off-regression points in Figure 4 are plotted.

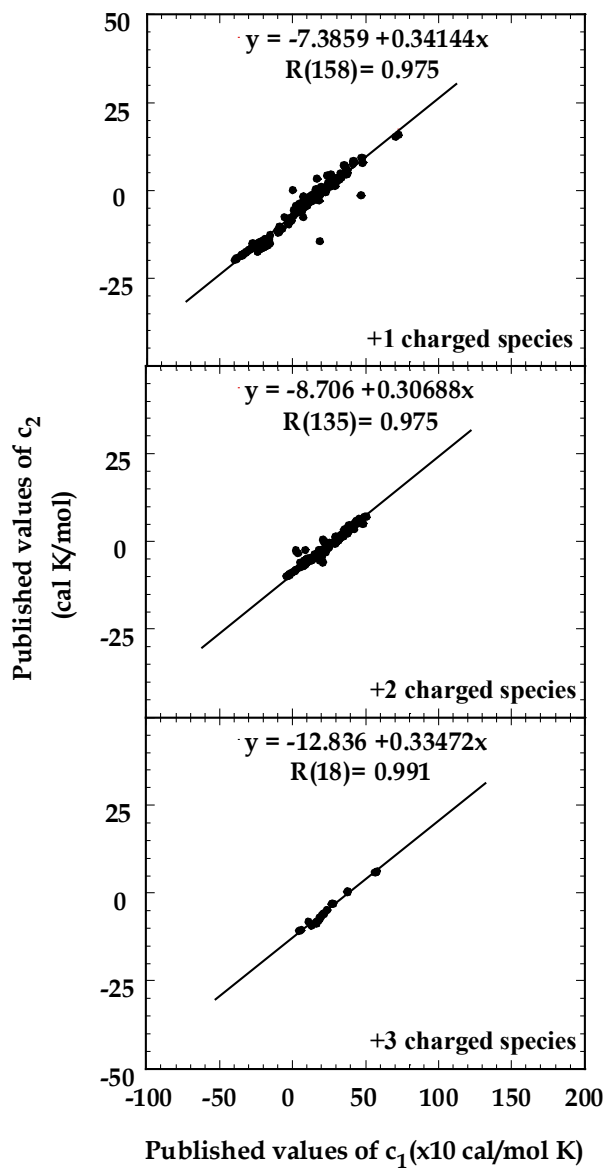


Figure 6: Published values of c_2 as a function of published values of c_1 for the positively charged dissolved aqueous species.

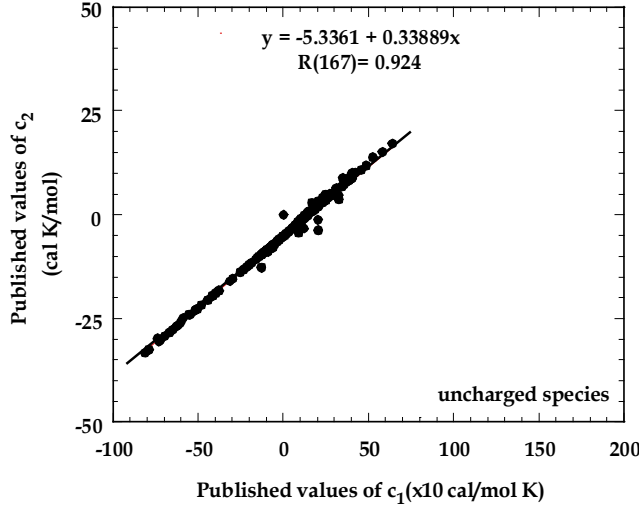


Figure 7: Published values of c_2 as a function of published values of c_1 for the uncharged dissolved aqueous species.

4. a_1 and c_1 as Functions of Standard State Entropy, Charge, and Species Type

Shock et al. (1997) and Sverjensky et al. (1997) show how linear relationships between entropy, volume, and heat capacity can be used in prediction. Because a_1 and c_1 are defined as the intrinsic volume and intrinsic heat capacity respectively (Helgeson and Kirkham, 1976), they should be linearly related to entropy.

We now show that a_1 and c_1 are related to standard state entropy for common structural groups of aqueous species. We show that grouped by species type and charge the intrinsic volume (a_1) and intrinsic heat capacity (c_1) of any aqueous species are simple functions of standard state entropy, species charge, and species type. All relationships are of the form:

$$a_i = a_{i0} + a_{i1}S^o \quad (62)$$

and

$$c_i = c_{i0} + c_{i1}S^o, \quad (63)$$

where the regression coefficients (subscripted $i0$ and $i1$) depend on the anion, cation, the standard state partial molal entropy (S^o) of the species charge. These coefficients and the R^2 values are listed in Table 1. Plots of all regressions are provided in Figures 10-23.

The correlations summarized in (62) and (63) are useful for two reasons. First, they allow the estimation of the revised-HKF equation of state coefficients for any aqueous species provided we know its standard state entropy, its charge, and its structural type. We can, therefore, easily complete existing databases by filling in the missing data with estimated data. Second, if the equations are used for all species, the entire data set will be self-consistent. Finally, the fact that the relationships are linear suggests that the

fundamental chemistry of the aqueous species underlies the correlations. The correlations summarize large amounts of data in a way that should facilitate the development and testing of fundamental quantum mechanical models of aqueous solvation.

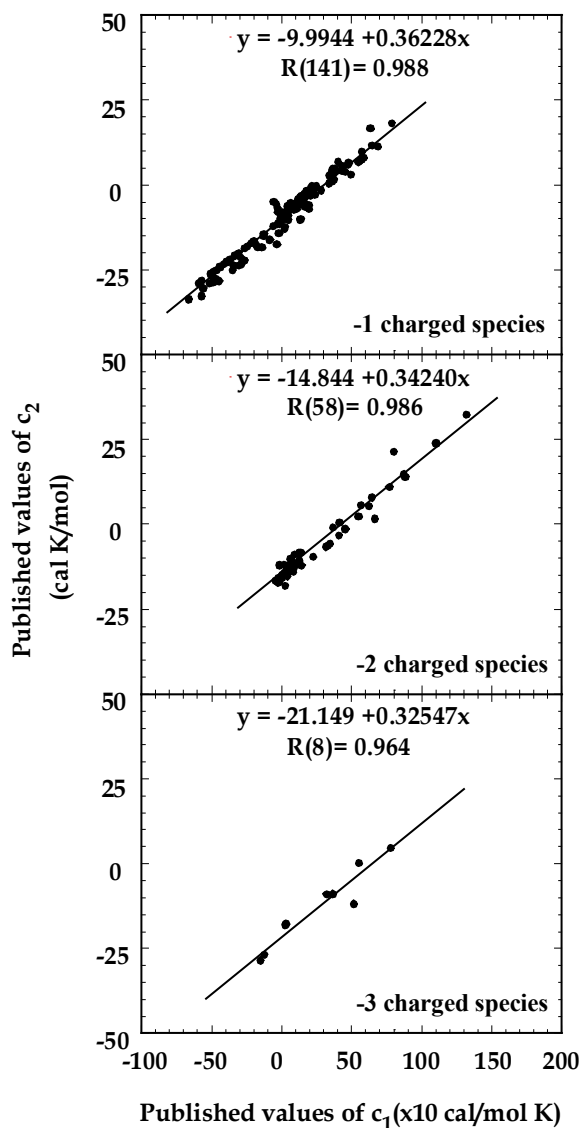


Figure 8: Published values of c_2 as a function of published values of c_1 for the negatively charged dissolved aqueous species.

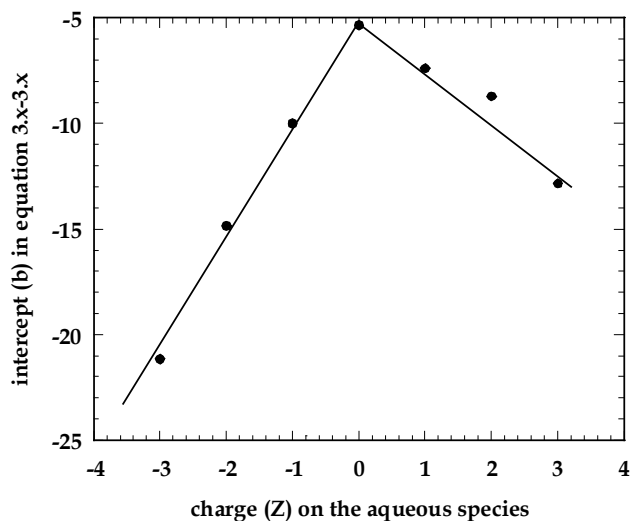


Figure 9: The intercepts of the equations describing c_2 as a function of c_1 as a function of the charge on the dissolved aqueous species.

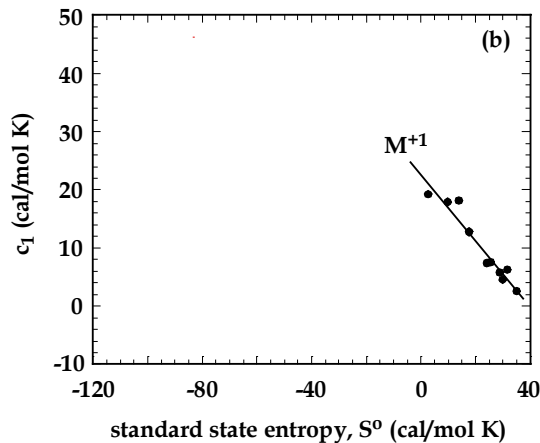
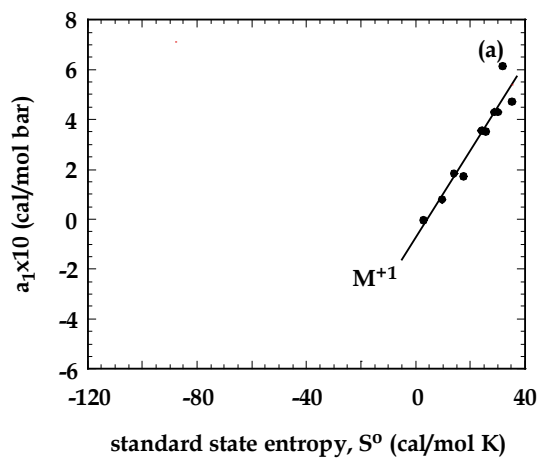


Figure 10. a_1 and c_1 regressions for +1 charged metal cations, M^{+1}

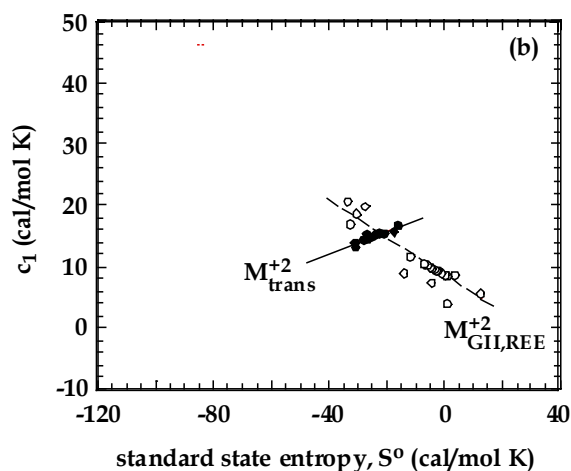
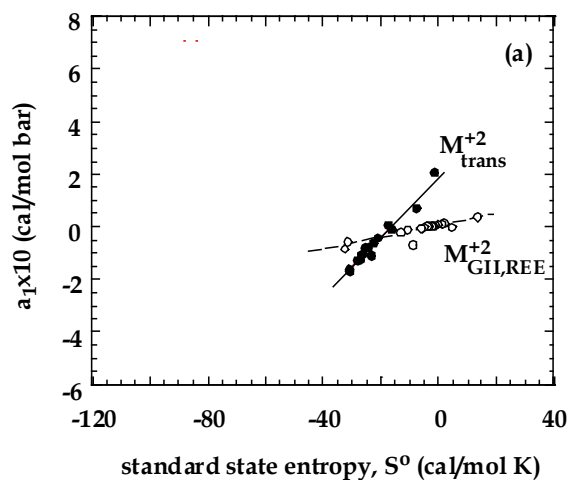


Figure 11: a_1 and c_1 regressions for charge +2 transition metal cations and Group II/REE cations (open circles), and +2 transition metal cations (closed circles).

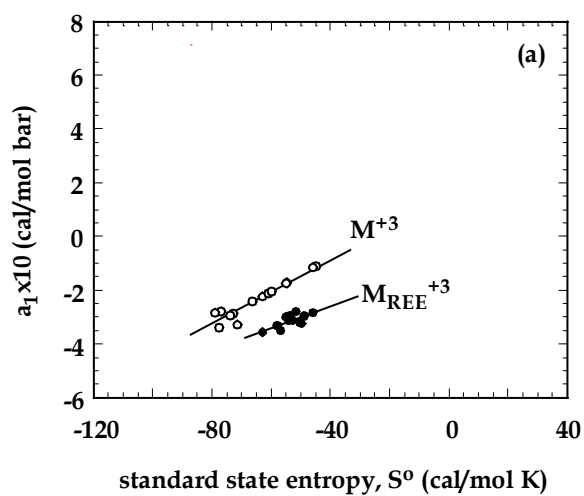


Figure 12a: a_1 regressions for simple +3 metal cations (open circles), and +3 REE cations (closed circles).

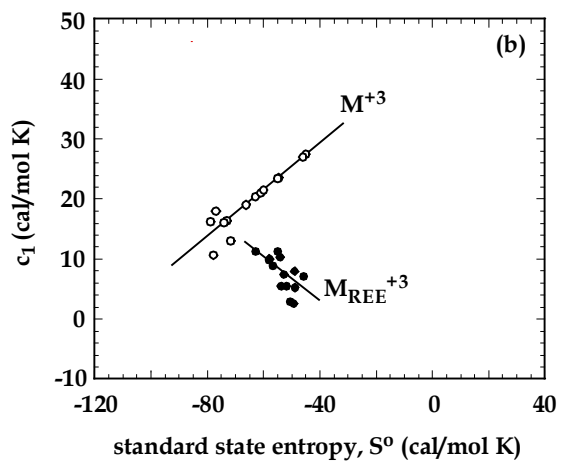


Figure 12b: c_1 regressions for simple +3 metal cations (open circles), and +3 REE cations (closed circles).

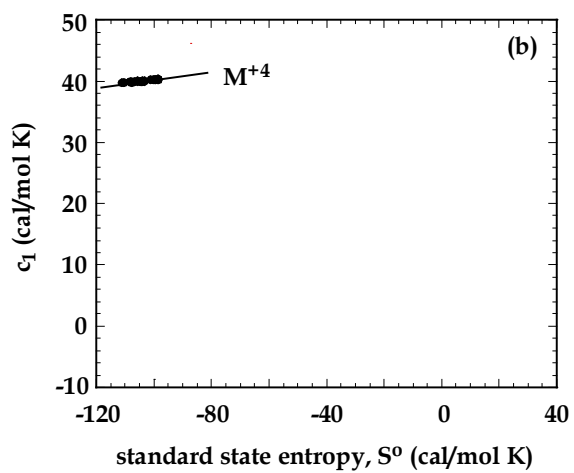
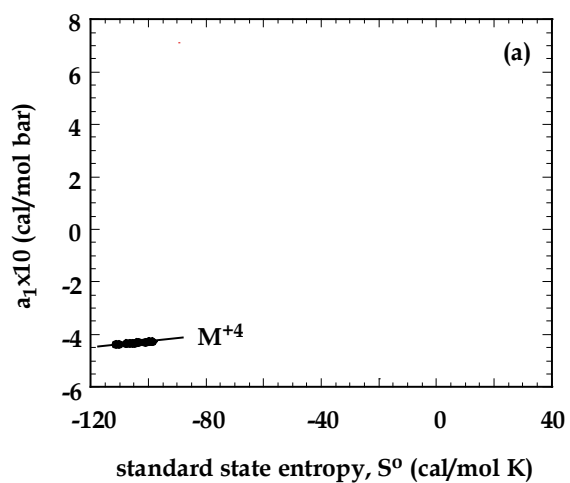


Figure 13: a_1 and c_1 regressions for simple +4 cations.

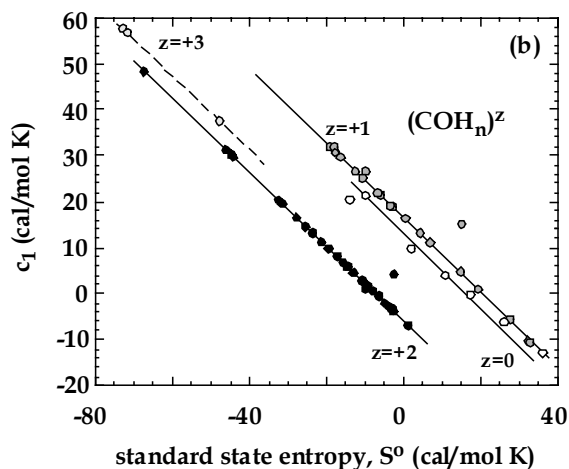
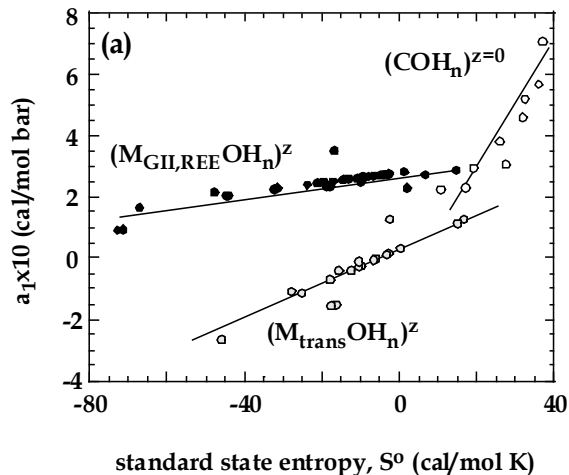


Figure 14: a_1 and c_1 regressions for hydroxide aqueous complexes. c_1 regressions do not depend on cation type; a_1 regressions do depend on type. z is charge, n is the number of hydroxide ions. a_1 regressions do not depend on charge or the number of hydroxide ions; c_1 regressions depend on charge (and therefore on n).

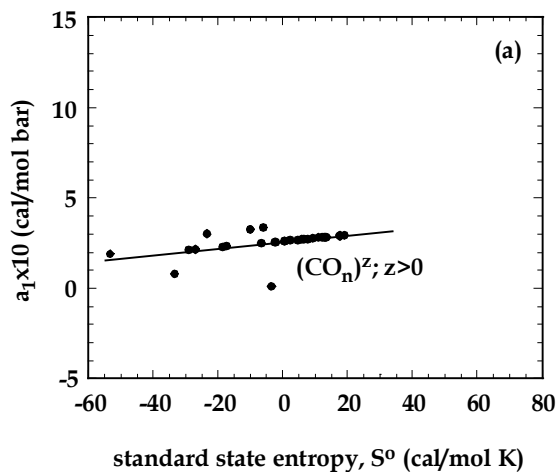


Figure 15a: a_1 regression for simple oxide aqueous complexes with positive charge. C is a simple cation, O is oxygen, n is the number of oxygen atoms in the complex. For these regressions n must be such that $z > 0$ for the chosen cation.

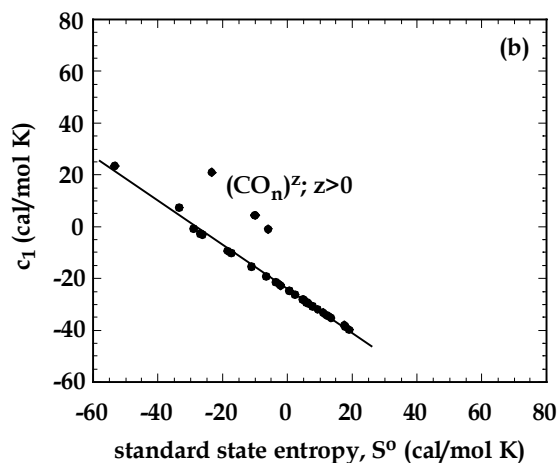


Figure 15b: c_1 regression for simple oxide aqueous complexes with positive charge. C is a simple cation, O is oxygen, n is the number of oxygen atoms in the complex. For these regressions n must be such that $z > 0$ for the chosen cation.

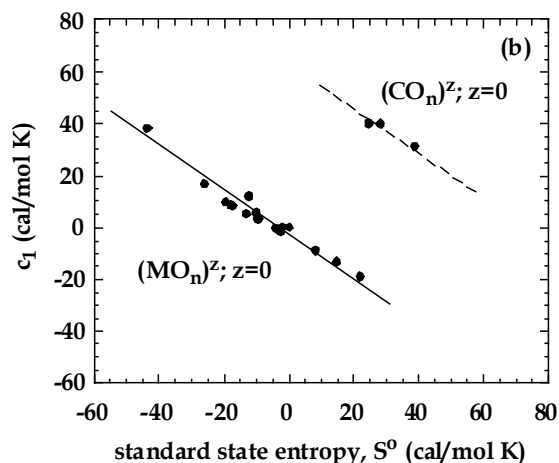
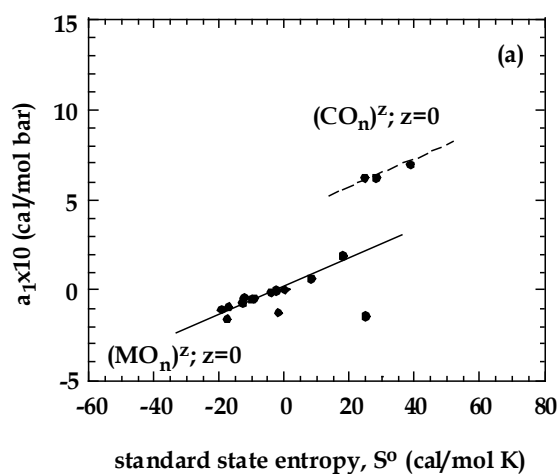


Figure 16: a_1 and c_1 regressions for uncharged oxide aqueous complexes. C indicates a simple cation, O oxygen, n the number of oxygen atoms in the complex. For these regressions n must be such that $z = 0$ for the selected cation.

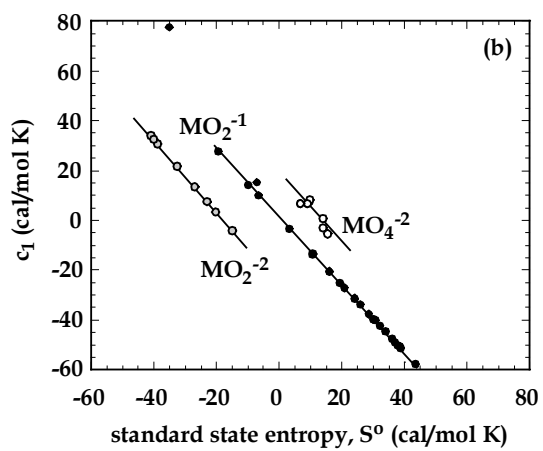
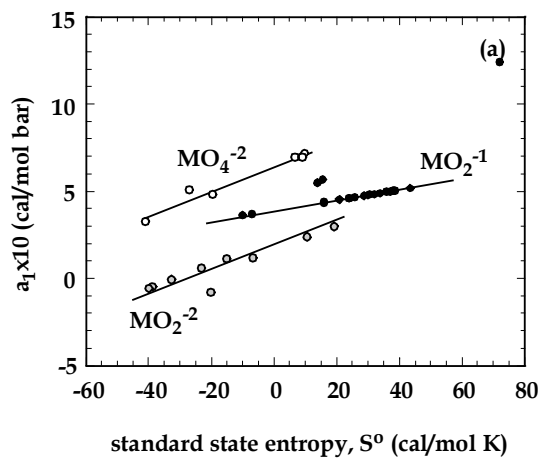


Figure 17: a_1 and c_1 regressions for negatively charged metal oxide aqueous complexes with 2 or 4 oxygen atoms in the complex.

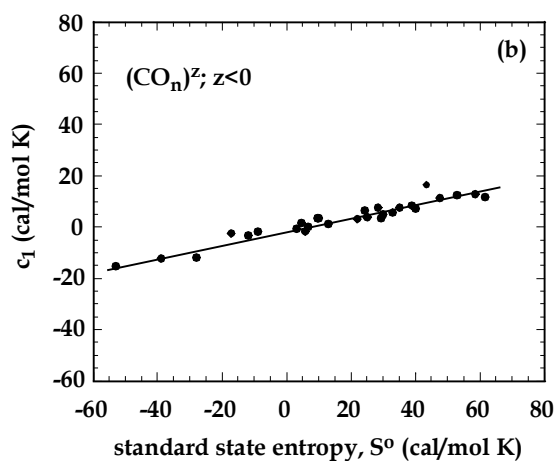
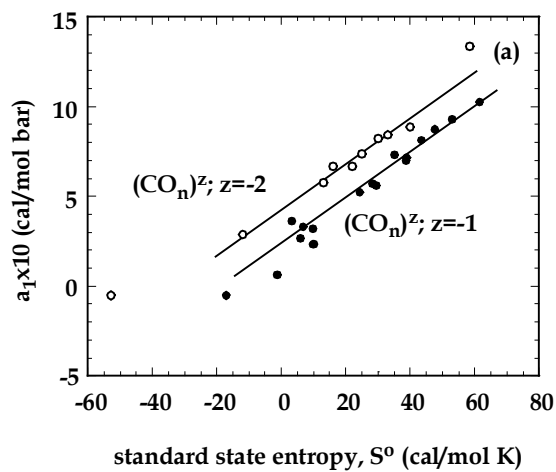


Figure 18: a_1 and c_1 regressions for simple cation aqueous oxide complexes of negative charge.

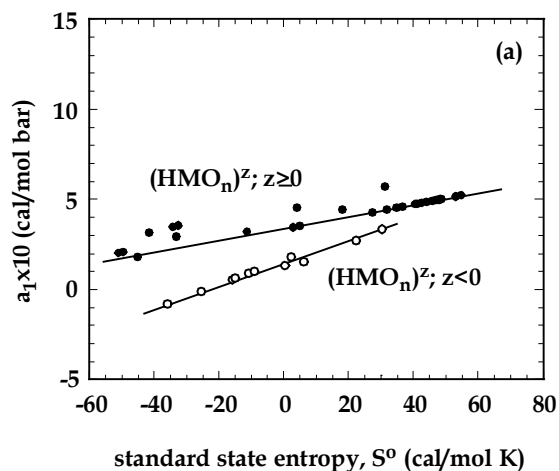


Figure 19: a_1 and c_1 regressions for protonated metal oxide aqueous complexes. a_1 and c_1 regressions are different for complex charge <0 and >0 or $=0$. c_1 regressions for $z = -2$ differ from all other charges (positive or negative).

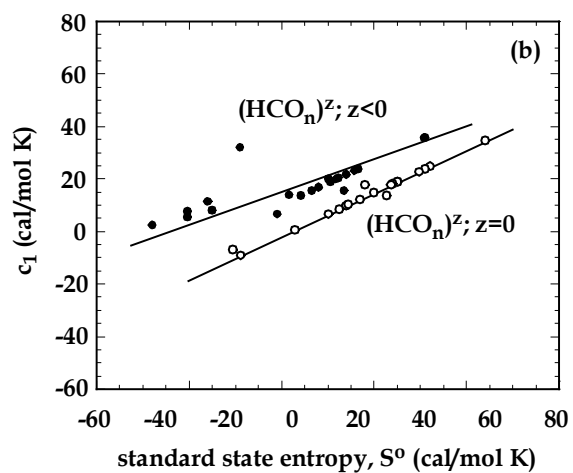
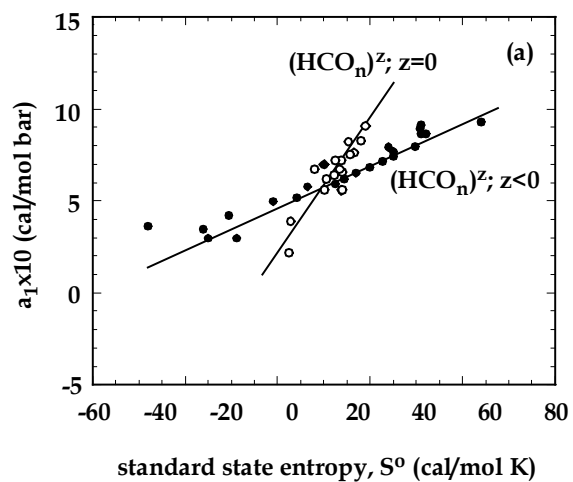


Figure 20: a_1 and c_1 regressions for protonated simple uncharged and negatively charged oxide aqueous complexes.

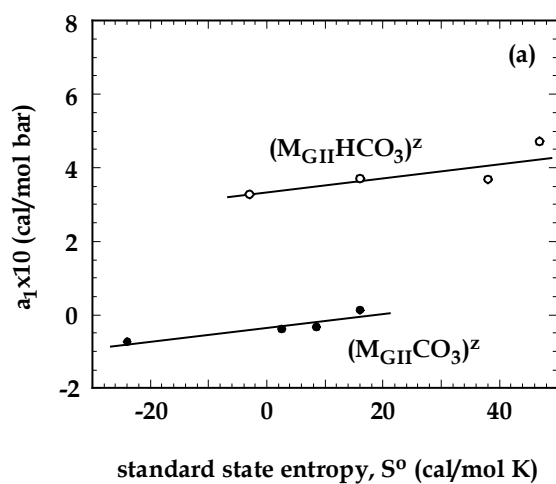


Figure 21a: a_1 regressions for carbonates and bicarbonates depend on cation type but not complex charge.

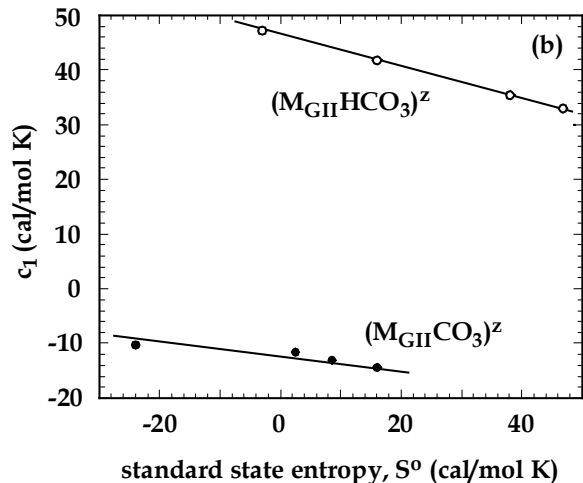


Figure 21b: c_1 regressions for carbonates and bicarbonates depend on cation type but not complex charge.

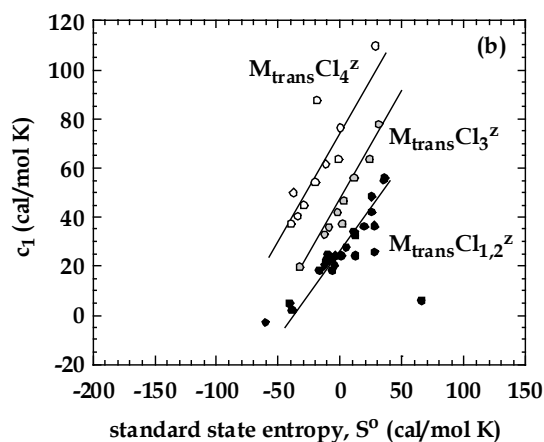
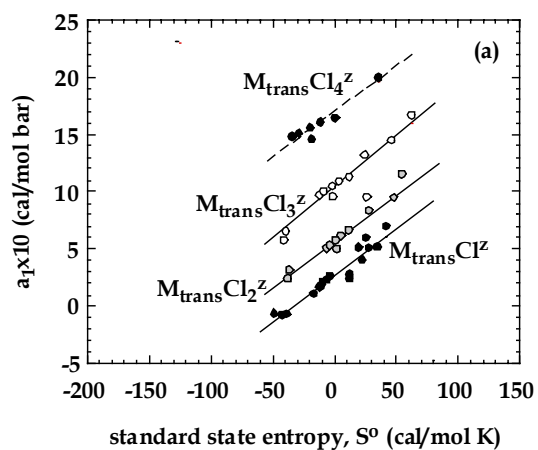


Figure 22: a_1 and c_1 regressions for transition metal chloride complexes depend on the number of Cl atoms in the complex but not on complex charge.

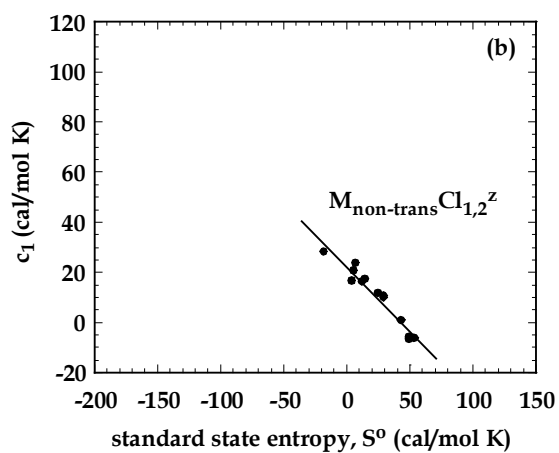
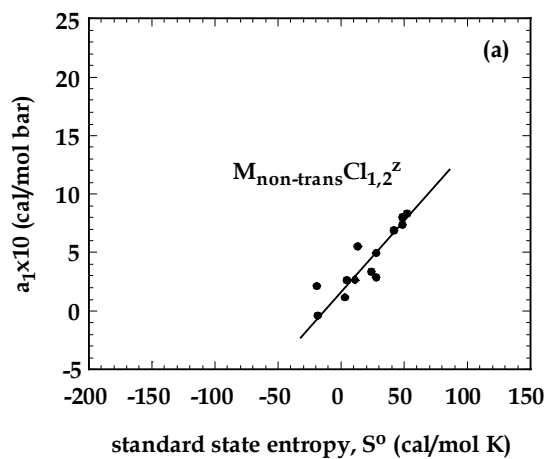


Figure 23: a_1 and c_1 regressions for non-transition metal chloride complexes with one of two chlorine atoms in the complex (complexes with order higher than this rarely form) are independent of complex charge.

Table 1: A compilation of the coefficients for the linear regressions presented in the text. M = metal cation, C = cation, m = number of cations, n = number of anions, z = charge of the complex.

$$a_i = a_{10^+} a_{11} S^o; R_a(n);$$

$$c_i = c_{10^+} c_{11} S^o; R_c(n).$$

	a_{10}	a_{11}	c_{10}	c_{11}	$R_a(n)$	$R_c(n)$
simple cations						
M^{+1}	-0.478	0.164	22.76	-0.572	0.962(10)	0.967(10)
$M_{\text{GII,REE}}^{+2}$	0.069	0.023	8.65	-0.346	0.914(20)	0.869(20)
M_{trans}^{+2}	2.080	0.122	19.18	0.174	0.983(13)	0.918(13)
M^{+3}	1.610	0.061	45.26	0.398	0.957(14)	0.926(14)
M_{REE}^{+3}	-0.860	0.043	-12.137	-0.347	0.800(15)	0.667(15)
M^{+4}	-3.450	0.008	45.01	0.048	0.995(18)	0.989(18)
hydroxides						
$(\text{COH}_n)^{z=0}$	1.080	0.127	11.15	-0.668	0.913(9)	0.993(9)
$(M_{\text{GII,REE}}\text{OH}_n)^z$	2.790	0.017			0.988(33)	
$(M_{\text{trans}}\text{OH}_n)^z$	0.642	0.059			0.992(23)	
$(\text{COH}_n)^{z=+1}$			17.32	-0.748		0.990(20)
$(\text{COH}_n)^{z=+2}$			-5.88	-0.807		0.998(26)
$(\text{COH}_n)^{z=+3}$			-0.977	-0.807		0.999(3)
oxides						
$(\text{MO}_n)^{z>0}$	2.62	0.017	-24.37	-0.81	0.977(26)	0.983(26)
$(\text{CO}_n)^{z=0}$	3.56	0.096	63.09	-0.80		
$(\text{MO}_n)^{z>0}$	0.59	0.096	-2.62	-0.80	0.984(14)	0.992(14)
$(\text{MO}_2)^{z=-1}$	3.92	0.029	2.24	-1.39	0.979(23)	0.988(23)
$(\text{MO}_2)^{z=-2}$	2.18	0.069	-26.37	-1.47	0.991(8)	0.999(8)
$(\text{MO}_4)^{z=-2}$	6.57	0.054	16.6	-1.37	0.989(6)	0.867(6)
$(C_m\text{O}_n)^{z=-1}$	1.77	0.143			0.988(17)	
$(C_m\text{O}_n)^{z=-2}$	3.74	0.136			0.986(10)	
$(C_m\text{O}_n)^{z<0}$			-1.12	0.246		0.983(27)
$(\text{HM}_m\text{O}_n)^{z<0}$	1.52	0.062			0.997(11)	
$(\text{HM}_m\text{O}_n)^{z>0}$	3.36	0.034			0.986(29)	
$(\text{HM}_m\text{O}_n)^{z=-2}$			3.41	1.574		0.980(33)
$(\text{HM}_m\text{O}_n)^{z\neq-2}$			74.13	1.274		0.821(7)
$(\text{HM}_m\text{O}_n)^{z=0}$	1.12	0.141	-17.32	0.790	0.875(23)	0.756(23)
$(\text{HM}_m\text{O}_n)^{z<0}$	4.14	0.085	6.15	0.766	0.889(18)	0.992(18)
carbonates						
$(M_{\text{GII}}\text{CO}_3)^z$	-0.345	0.019	-11.909	-0.074	0.990(4)	0.985(18)
bicarbonates						
$(M_{\text{GII}}\text{HCO}_3)^z$	3.39	0.010	46.40	-0.294	0.977(4)	0.999(4)
chlorides						
$(M_{\text{trans}}\text{Cl})^z$	2.73	0.080	27.99	0.650	0.887(18)	0.845(29)
$(M_{\text{trans}}\text{Cl}_2)^z$	5.54	0.079	27.99	0.650	0.903(11)	0.845(29)
$(M_{\text{trans}}\text{Cl}_3)^z$	10.26	0.093	45.39	0.956	0.937(18)	0.991(18)
$(M_{\text{trans}}\text{Cl}_4)^z$	17.01	0.075	77.37	1.003	0.955(18)	0.889(18)
$(M_{\text{GII}}\text{Cl}_4)^z$	1.67	0.118	21.76	-0.503	0.867(12)	0.970(12)

E. Predicting Brine Chemistry

Figure 24 shows scatter plots of major cations measured at two locations: Calcasieu Parish, LA (Hanor, 1994) and in the Moore-Sams-Morganza Gas Field in the Tuscaloosa Trend, LA (Ross et al., 1994). The lines through the data are the equilibrium concentrations of the major cations predicted using the method outlined in the previous sections. The solid lines represent the concentrations of the major cations in equilibrium with albite, calcite, dolomite, K-feldspar, Mg-chlorite, muscovite, and quartz at 100°C. Both Hanor (1994) and Smith and Ehrenberg (1989) have suggested this buffer as being mineralogically representative of the sediments in basins. The dashed lines represent the concentrations of the major cations in equilibrium with the same buffer with kaolinite in place of muscovite. This is the same as the Buffer 1 suite of minerals we shall use later, except that iron sulfide minerals are omitted. Changes in the buffer could fit the data more exactly. The agreement between the calculated and measured concentrations indicates that the pore fluids at these locations are in equilibrium with the sediment minerals. It also verifies the suitability of our Buffer 1 set of minerals for predicting brine chemistry in the Gulf of Mexico.

F. Inorganic Alteration by Brine Movement through Seals

We are now in a position to calculate the inorganic alteration caused by the movement of aqueous fluids through basin seals. We will calculate flow through a series of hypothetical sea types. We first define the pressure and temperature profiles through these seals, then estimate the mass flux of brine through a top seal, and finally calculate the alteration this flux will produce for two mineral buffers and several brine salinities. We reach three major conclusions: (1) fluid flow is necessary to explain the magnitude of observed inorganic alteration, (2) alteration is intensified when temperature and pressure gradients increase (e.g., in the pressure transition zone) and when the fluids have higher salinity, and (3) stepped pressure gradients in the pressure transition zone may explain the diagenetic banding often observed in pressure transition zones.

1. *P-T* Gradients in Sedimentary Basins

The pressure gradients typically observed in sedimentary basins are shown in Figure 25. Hydrostatic or “normal” pressure gradients range from 98-105 bar km⁻¹. Normal temperature gradients generally range from 15-50°C km⁻¹ (North, 1990). In most active sedimentary basins, the temperature and pressure gradients increase dramatically below a certain depth called the “top of overpressure.” The top of overpressure is underlain by a pressure transition zone <0.1 to ~0.5 km thick (Hunt, 1990). Through this pressure transition zone, the pressure increases sharply to ~100-500 bar greater than hydrostatic. The geothermal gradient also increases sharply at the top of overpressure (to about 50-90°C km⁻¹ in the US Gulf Coast) (North, 1990).

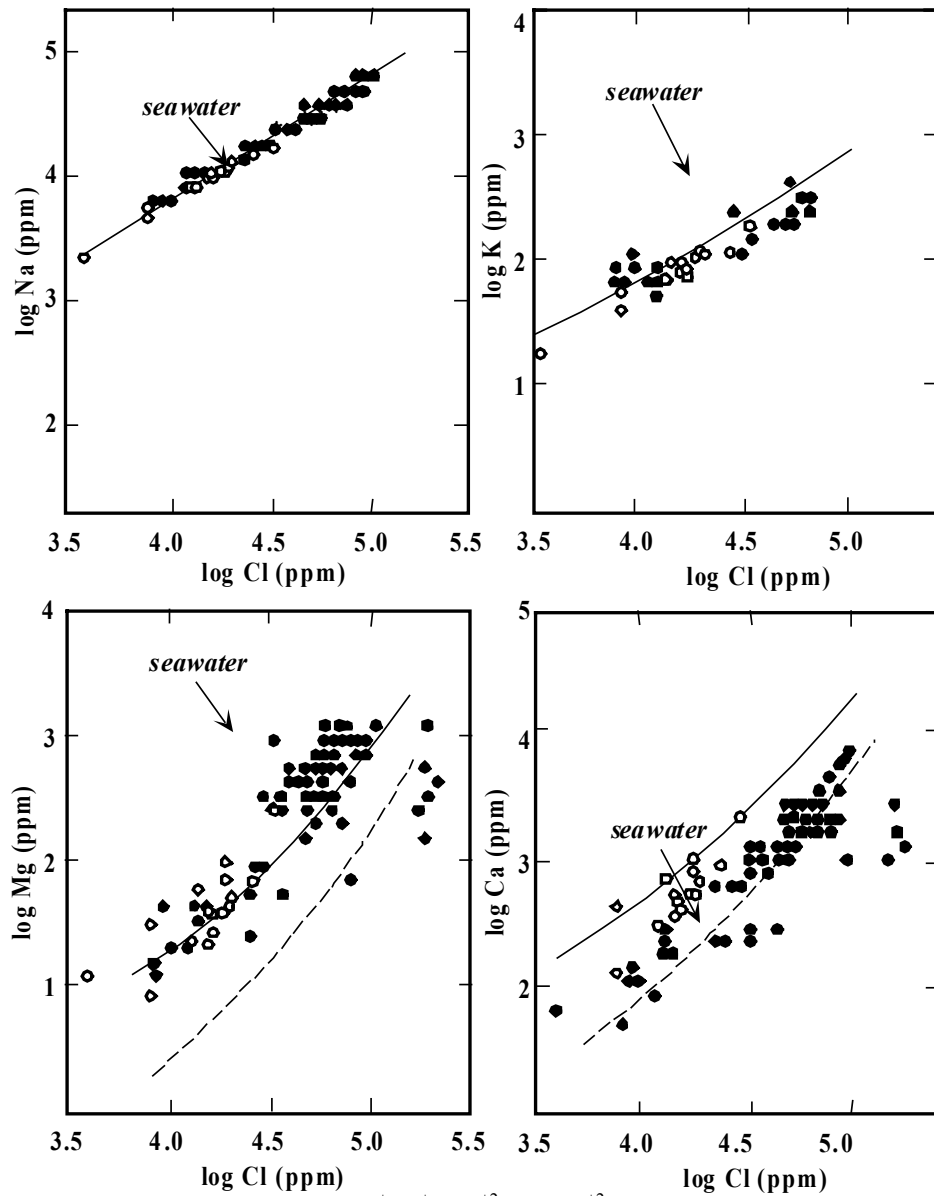


Figure 24: Data points: total dissolved Na^+ , K^+ , Mg^{+2} , and Ca^{+2} as a function of dissolved chloride measured in Calcasieu Parish, SW Louisiana (black circles; after Hanor, 1994) and the Moore-Sams-Morganza gas field Tuscaloosa Trend, LA (open circles; after Ross et al. 1994). Solid and dashed curves show chemistry predicted at 100 C by mineral buffers described in the text.

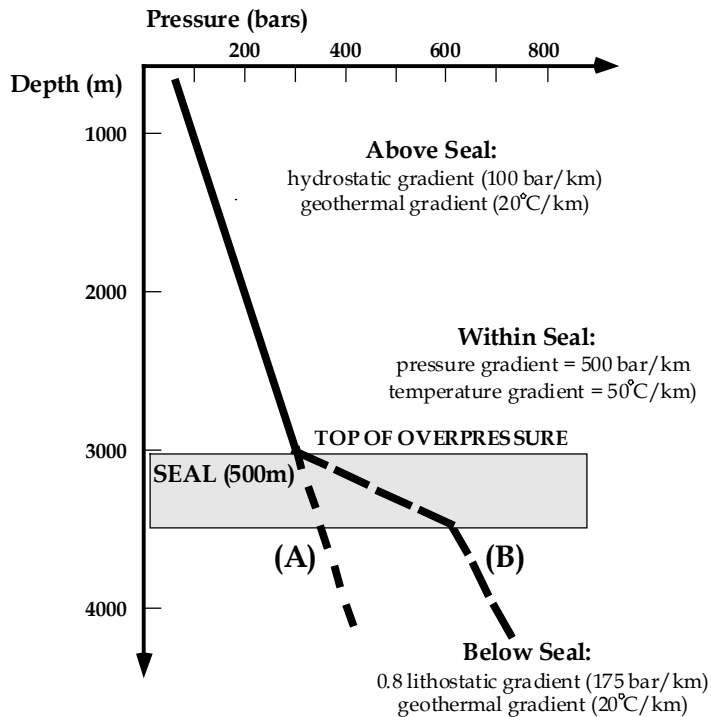


Figure 25: (A) Hydrostatic-normal geothermal profile and (B) Basin profile for a basin that becomes overpressured at 3 km depth.

Two generalized temperature-pressure profiles are used in the alteration calculations performed in this study: (1) a hydrostatic-geothermal gradient, $\partial T / \partial z = 20^{\circ}\text{C km}^{-1}$; $\partial P / \partial z = 100 \text{ bar km}^{-1}$ (denoted “A” in Figure 25) and (2) an overpressured temperature-pressure profile (denoted “B” in Figure 25). The pressure and temperature gradients in both profiles are the same (hydrostatic-geothermal) above the top of overpressure. In the hydrostatic geothermal profile, these vertical gradients of P and T remain unchanged as a function of depth. In the overpressured profile, the temperature and pressure gradients increase abruptly at the top of overpressure ($\partial T / \partial z = 50^{\circ}\text{C km}^{-1}$; $\partial P / \partial z = 500 \text{ bar km}^{-1}$ over a short distance). Below the top of overpressure, the temperature gradient of the overpressured profile returns to $20^{\circ}\text{C km}^{-1}$, but the pressure gradient is 0.8 lithostatic ($\partial P / \partial z = 175 \text{ bar km}^{-1}$). The methods summarized earlier in this report are used to compute the required thermodynamic parameters of minerals and aqueous species so that the mineralogical alteration caused by vertical fluid flow can be calculated.

2. Diagenetic Alteration

When sediments are deposited on the sea floor, they are saturated with seawater and shortly after burial have a porosity of between 30-40%. During burial, the sediments are diagenetically altered as the connate seawater equilibrates chemically with the minerals in the sediments. In this section, we calculate this diagenetic alteration by computing the change in seawater composition that occurs as it equilibrates with the sediments. We also compute the mineralogical changes in the sediment. By calculating the diagenetic alteration, we obtain the “background” alteration against which to compare the alteration we predict will occur due to the movement of fluids through the basin. The diagenetic

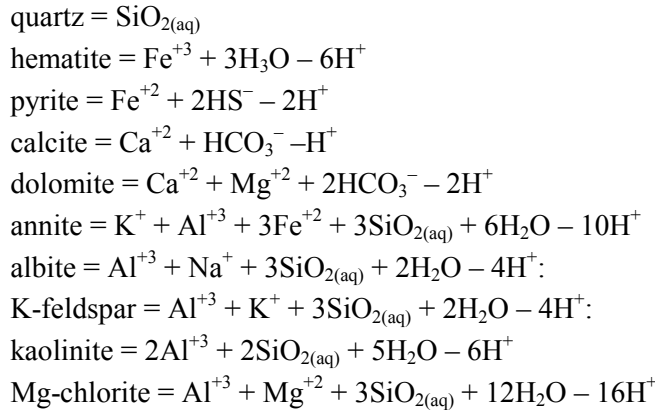
alteration estimates are minimum estimates because we do not consider diffusion of ions from the ocean water into the shallow sediment column. This is acceptable because our purpose is to provide an alteration benchmark against which we can assess fluid flow-related alteration.

The composition of seawater (Table 2) gives us the total concentration of each of the basis species in the pore fluid before the minerals in the sediments have buffered the fluid composition. We can calculate the total basis species composition of the fluid in equilibrium with a mineral buffer at 0.25 km (25°C, 25 bar), 1.5 km (50°C, 150 bar), and 2.75 km (75°C, 275 bar). The difference between the composition of seawater and the composition of these pore waters in equilibrium with the mineral buffer allows us to calculate the chemical flux to the sediment minerals and the change in mineralogy that will result from this flux (see equations (1)-(3) above). The mineral buffer we choose to calculate diagenetic alteration is: quartz, hematite, pyrite, calcite, dolomite, annite, albite, K-feldspar, kaolinite, and Mg-chlorite. These minerals are expressed in terms of the following basis species: Al^{+3} , Ca^{+2} , Fe^{+2} , Fe^{+3} , H_2O , H^+ , HCO_3^- , HS^- , K^+ , Mg^{+2} , Na^+ , SiO_2 . The reactions by which our buffer minerals are dissolved to these basis species are given in Table 3.

Table 2: Composition of seawater (Drever, 1982).

Dissolved Species	Concentration, C_i (g/kg)	Concentration, C_i (mol/kg)
Cl^-	19.354	5.46×10^{-1}
Na^+	10.77	4.68×10^{-1}
K^+	0.399	1.02×10^{-2}
Ca^{+2}	0.4121	1.03×10^{-2}
Mg^{+2}	1.29	5.31×10^{-2}
$\text{Fe}^{+2} + \text{Fe}^{+3}$	2×10^{-6}	3.58×10^{-8}
O_2	1×10^{-5} - $6 \cdot 10^{-3}$	3.12×10^{-7} - 1.88×10^{-4}
SO_4^{-2}	2.712	2.82×10^{-2}
HCO_3^-	0.1424	2.33×10^{-3}
SiO_2	5×10^{-4} -0.01	8.32×10^{-6} - 1.56×10^{-4}
Al^{+3}	2×10^{-6}	7.41×10^{-8}

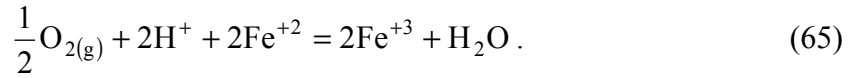
Table 3: The minerals for the Buffer 1 assemblage expressed in terms of our basis species.



The composition of seawater also needs to be expressed in terms of our basis species. To achieve this we make several assumptions. First, because there is quite a range of silica concentrations ($8.32 \times 10^{-6} - 1.56 \times 10^{-4} \text{ mol kg}^{-1}$) we assume that seawater is in equilibrium with quartz. The equilibrium concentration of $\text{SiO}_{2(\text{aq})}$ given by the solubility product of quartz at *STP* ($T = 25^\circ\text{C}$, $P = 1 \text{ bar}$):

$$K_{\text{quartz}} = [\text{SiO}_{2(\text{aq})}] = 10^{-4} \text{ mol kg}^{-1}. \quad (64)$$

Next we distribute the iron in seawater ($2 \mu\text{g kg}^{-1}$) between Fe(II) and Fe(III). We do this by assuming that Fe(II) and Fe(III) are in equilibrium with each other and with oxygen in solution. The redox equation that describes this equilibrium is:



The equilibrium condition at 25°C is:

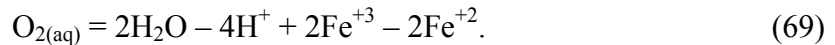
$$K_{(65)} = \frac{[\text{Fe}^{+3}]^2}{[\text{Fe}^{+2}]^2 [\text{H}^+]^2 P_{\text{O}_2}^{1/2}} = 10^{15.53}. \quad (66)$$

The equilibrium Fe(III)/Fe(II) ratio is

$$\left[\frac{\text{Fe}^{+3}}{\text{Fe}^{+2}} \right] = \left[10^{15.53} [\text{H}^+]^2 P_{\text{O}_2}^{1/2} \right] \quad (67)$$

Reported seawater oxygen concentrations range between 3.12×10^{-7} and $1.88 \times 10^{-4} \text{ mol kg}^{-1}$ and correspond to equilibrium with a partial pressure of oxygen of P_{O_2} is 1×10^{-5} to 0.006 atm . Assuming that $P_{\text{O}_2} = 0.006 \text{ atm}$ and that the pH of seawater is 8 gives an iron ratio $[\text{Fe}^{+3}]/[\text{Fe}^{+2}]$ of 0.162. Distributing the $2 \mu\text{g kg}^{-1}$ of iron in seawater using this ratio, we find Fe(II) = $1.72 \mu\text{g kg}^{-1}$ and Fe(III) = $0.28 \mu\text{g kg}^{-1}$.

Finally we must represent the molal concentrations of all species in seawater in terms of our chosen basis species. The reactions used to do this are:



with our mineral buffer at various depths are listed in Table 4. The hydrostatic-geothermal gradient defined in Figure 25 is assumed in these calculations.

In calculating diagenetic alteration, we also need to consider the mass of seawater that is available to react with the sediments. Every cubic centimeter of buried sediment contains approximately 0.3 cm^3 of water (assuming that the porosity of the sediments is $\sim 30\%$)

and 0.7 cm^3 of sediment. Assuming that the density of water is $\sim 1 \text{ g cm}^{-3}$ and the density of the sediment is $\sim 2.7 \text{ cm}^{-3}$, 0.3 grams of connate pore fluid (seawater) are available to equilibrate with 1.89 grams of sediment. This gives us a water-rock mass ratio of 0.16 grams of water per gram of sediment.

The mineralogical alteration caused by the equilibration of seawater with the sediments at 0.25, 1.50, and 2.75 km depth is given in Table 5 and plotted in Figure 26. As the connate seawater comes into equilibrium with the sediments at 25°C , hematite, pyrite, calcite, albite, K-feldspar, and Mg-chlorite precipitate at the expense of quartz, dolomite, annite, and kaolinite. If seawater reaches equilibrium with the sediments at 50°C or 75°C , dolomite is precipitated instead of calcite and Mg-chlorite. Alteration intensity is a few tenths of a weight percent.

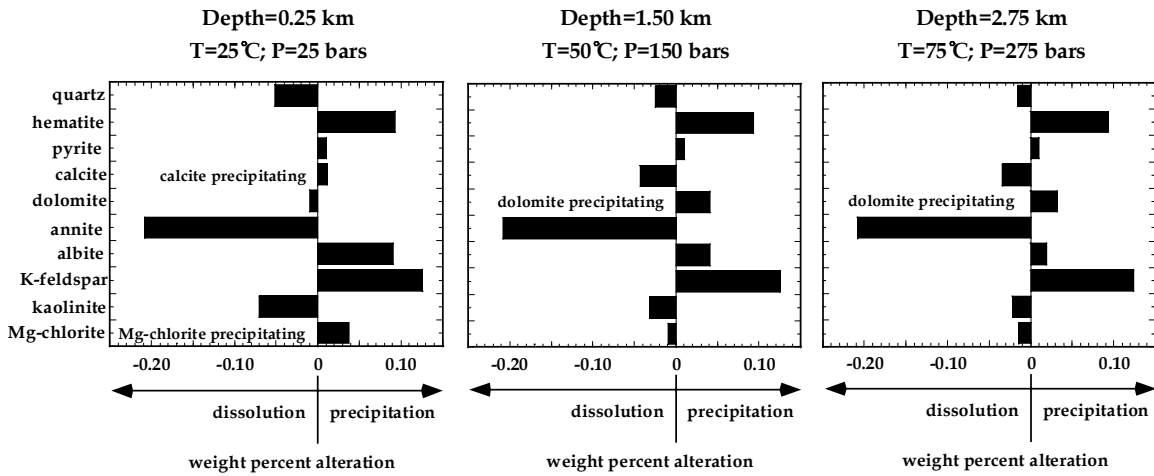


Figure 26: Mineral alteration (in wt %) that will be produced if pore fluids initially of seawater composition chemically equilibrate with sediment minerals at various depths.

Table 4: The change in total concentration of basis species (sum of species and all complexes which contain it) when seawater equilibrates with the Buffer 1 mineral assemblage at the P and T which occur at 0.25, 1.50, and 2.75 km depth under hydrostatic conditions and a $20^\circ\text{C}/\text{km}$ temperature gradient (Figure 25). C_n is the equilibrium fluid composition at P and T ; $C_n = C_n - C_{\text{seawater}}$ is the change in composition relative to seawater.

	C_i (at 25°C)	C_1		C_2		C_3	
	seawater (mol/kg)	(at 0.25 km)	$C_{1, \text{sw}}$	(at 1.50 km)	$C_{2, \text{sw}}$	(at 2.75 km)	$C_{3, \text{sw}}$
Cl^-	5.46×10^{-1}	5.38×10^{-1}	-7.91×10^{-3}	5.37×10^{-1}	-8.91×10^{-3}	5.37×10^{-1}	-8.91×10^{-3}
Na^+	4.68×10^{-1}	4.07×10^{-1}	-6.15×10^{-2}	4.41×10^{-1}	-2.75×10^{-2}	4.56×10^{-1}	-1.25×10^{-3}
K^+	1.02×10^{-2}	3.59×10^{-4}	-9.85×10^{-3}	9.20×10^{-4}	-9.28×10^{-3}	1.96×10^{-3}	-8.24×10^{-3}
Ca^{+2}	1.03×10^{-2}	6.12×10^{-2}	-1.02×10^{-2}	4.53×10^{-2}	3.50×10^{-2}	3.80×10^{-2}	2.77×10^{-2}
Mg^{+2}	5.31×10^{-2}	4.17×10^{-3}	-4.89×10^{-2}	2.34×10^{-3}	-5.07×10^{-2}	1.59×10^{-3}	-5.15×10^{-2}
Fe^{+2}	-2.24×10^{-1}	4.68×10^{-6}	2.24×10^{-1}	4.89×10^{-6}	2.24×10^{-1}	5.53×10^{-6}	2.24×10^{-1}
Fe^{+3}	2.24×10^{-1}	3.24×10^{-8}	-2.24×10^{-1}	1.25×10^{-7}	-2.24×10^{-1}	2.76×10^{-7}	-2.24×10^{-1}
HS^-	2.82×10^{-2}	9.36×10^{-9}	-2.82×10^{-2}	4.49×10^{-8}	-2.82×10^{-2}	1.51×10^{-7}	-2.82×10^{-2}
HCO_3^-	2.33×10^{-3}	6.91×10^{-5}	-2.27×10^{-3}	1.57×10^{-4}	-2.18×10^{-3}	3.00×10^{-4}	-2.03×10^{-3}
SiO_2	1.00×10^{-4}	1.12×10^{-4}	1.20×10^{-5}	2.80×10^{-4}	1.80×10^{-4}	5.55×10^{-4}	4.55×10^{-4}
Al^{+3}	7.41×10^{-8}	3.22×10^{-8}	-4.19×10^{-8}	8.85×10^{-8}	1.44×10^{-8}	2.08×10^{-7}	1.34×10^{-7}

Table 5: The mineral alteration due to the equilibration of seawater with the Buffer 1 mineral assemblage (Table 3). (+) denotes precipitation; (-) denotes dissolution.

	$\text{gm}_{\text{alteration}}/\text{gm}_{\text{sed}}$ weight % per gm_{water} (W/R=0.16) per cm^3 sediment		$\text{gm}_{\text{alteration}}/\text{gm}_{\text{sed}}$ weight % per gm_{water} (W/R=0.16) per cm^3 sediment		$\text{gm}_{\text{alteration}}/\text{gm}_{\text{sed}}$ weight % per gm_{water} (W/R=0.16) per cm^3 sediment	
	0.25 km		1.50 km		2.75 km	
quartz	-3.21×10^{-3}	-0.051	-1.59×10^{-3}	-0.025	-9.63×10^{-4}	-0.015
hematite	$+5.79 \times 10^{-3}$	+0.093	$+5.79 \times 10^{-3}$	+0.093	$+5.79 \times 10^{-3}$	+0.093
pyrite	$+6.26 \times 10^{-4}$	+0.010	$+6.26 \times 10^{-4}$	+0.010	$+6.26 \times 10^{-4}$	+0.010
calcite	$+6.72 \times 10^{-4}$	+0.011	-2.68×10^{-3}	-0.043	-2.13×10^{-3}	-0.034
dolomite	-5.42×10^{-4}	-0.009	$+2.54 \times 10^{-3}$	+0.041	$+2.03 \times 10^{-3}$	+0.032
annite	-1.30×10^{-2}	-0.208	-1.30×10^{-2}	-0.208	-1.30×10^{-2}	-0.208
albite	$+5.71 \times 10^{-3}$	+0.091	$+2.55 \times 10^{-3}$	+0.041	$+1.16 \times 10^{-3}$	+0.019
K-feldspar	$+7.88 \times 10^{-3}$	+0.126	$+7.82 \times 10^{-3}$	+0.125	$+7.72 \times 10^{-3}$	+0.124
kaolinite	-4.36×10^{-3}	-0.070	-1.96×10^{-3}	-0.031	-1.37×10^{-3}	-0.022
Mg-chlorite	$+2.29 \times 10^{-3}$	+0.037	-5.45×10^{-4}	-0.009	-8.77×10^{-4}	-0.014

If we assume that the connate pore fluids reach equilibrium with the sediments by the time the temperature rises to 75°C (2.75 km), we can calculate the alteration due to further burial (the movement of the sediments up temperature and pressure gradients), assuming the geothermal-hydrostatic gradient in Figure 25 pertains and that the water-rock mass ratio remains 0.16. As the sediments are buried another 0.25 km (to 3.0 km) the temperature increases from 75 to 80°C and the pressure increases from 275 to 300 bars. The total change in equilibrium fluid composition over the 0.25 km interval is shown in Table 6. The change in the concentration of HS⁻ in the fluids as the sediments are buried is positive ($\Delta C_I = 4.78 \times 10^{-8}$); we should expect a slight dissolution of pyrite, for example. The alteration caused by burial from 2.75 to 3.00 km depth is shown in Table 7 and plotted in Figure 27. As the sediments are buried, quartz, annite, calcite, kaolinite, and Mg-chlorite precipitate and hematite, pyrite, dolomite, albite, and K-feldspar dissolve. The character of alteration due to burial of the sediments is nearly the reverse of that caused by the initial equilibration of the sediments with seawater, but is of much smaller magnitude ($\sim 10^{-8}$ wt %). The inorganic diagenetic alteration, caused by further burial after the connate seawater has equilibrated with the sediments, is *extremely* small.

Figure 28 shows the alteration that would be caused by burial of sediments beyond 3.0 km depth. The mineralogy of the alteration changes slowly with depth. For example, the percentage of albite dissolving decreases from 63% to 28% of the total dissolution. The intensity of the alteration declines.

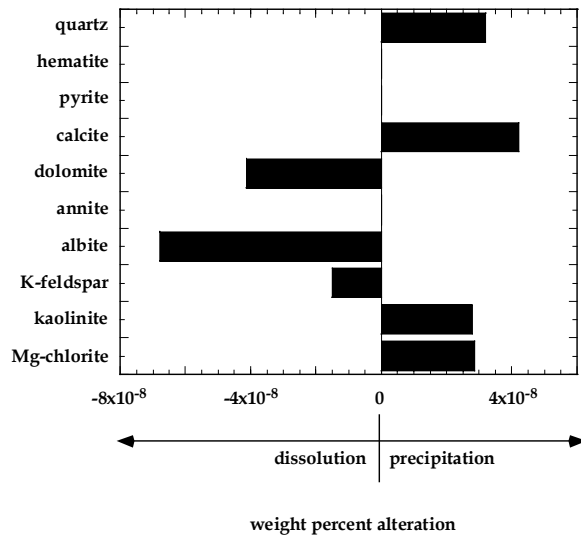


Figure 27: The weight percent mineral alteration caused to the burial from 2.75 to 3.0 km if pore waters chemistry is controlled by Buffer 1 minerals.

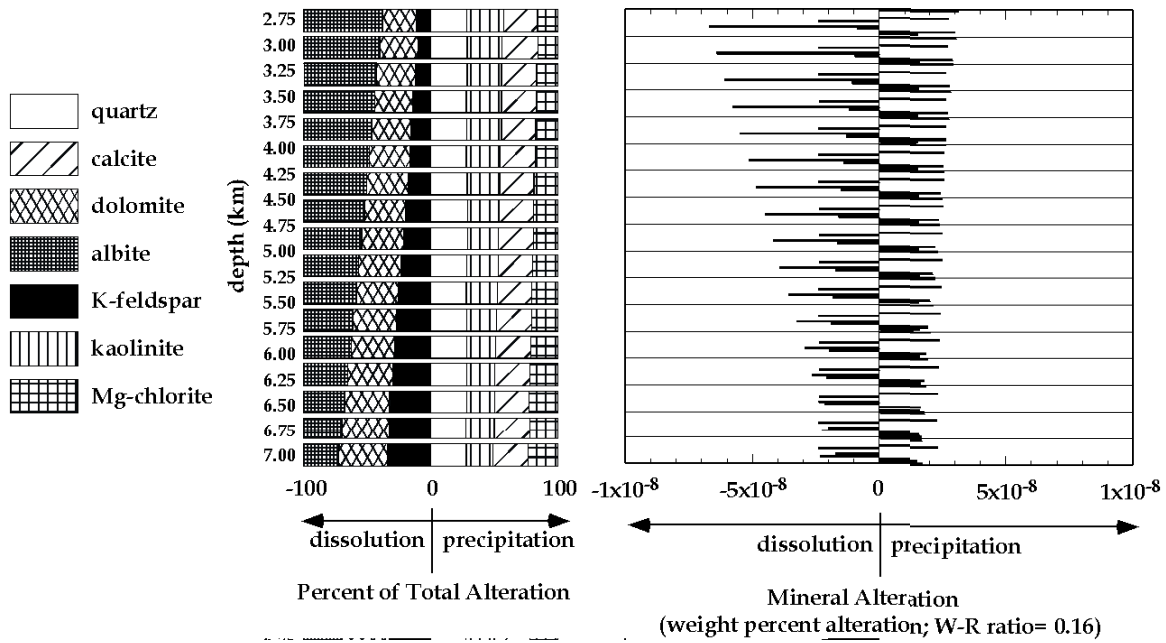


Figure 28: The percentage of minerals dissolved or precipitated, and the weight percent (of the total sediment mass) to successively greater depths due to continued sedimentation. Pore waters are always in equilibrium with Buffer 1 minerals (Table 3).

Table 6: The change in total basis species composition that occurs in a pore fluid which is in equilibrium with the Buffer 1 mineral assemblage when its host sediment is buried from 2.75 to 3.00 km depth in a hydrostatic environment with a temperature gradient of 20°C/km.

	C_i (at 0.25 km)	C_i (at 0.30 km)	C_i
Cl^-	5.37×10^{-1}	5.37×10^{-1}	1.06×10^{-5}
Na^+	4.58×10^{-1}	4.60×10^{-1}	2.16×10^{-3}
K^+	2.24×10^{-3}	2.55×10^{-3}	3.11×10^{-4}
Ca^{+2}	3.71×10^{-2}	3.60×10^{-2}	-1.12×10^{-3}
Mg^{+2}	1.51×10^{-3}	1.42×10^{-3}	-8.99×10^{-5}
Fe^{+2}	-5.70×10^{-6}	5.84×10^{-6}	1.43×10^{-7}
Fe^{+3}	3.17×10^{-7}	3.52×10^{-7}	3.50×10^{-8}
HS^-	1.93×10^{-7}	2.41×10^{-7}	4.78×10^{-8}
HCO_3^-	3.43×10^{-4}	3.88×10^{-4}	4.34×10^{-5}
SiO_2	6.26×10^{-4}	7.02×10^{-4}	7.16×10^{-5}
Al^{+3}	2.08×10^{-7}	2.49×10^{-7}	4.03×10^{-8}

The small weight percents predicted for diagenetic mineral alteration are generally not sufficient to explain the mineral alteration observed in sedimentary basins, which is commonly ~0.5-2 weight percent. Either more intense alteration must be produced by fluids moving through the basin, or the diagenetic alteration must be augmented by chemical diffusion from seawater, a possibility we will not pursue here.

Tables 6 and 7 and Figures 29 and 30 show the diagenetic alteration that will occur when equilibrated connate water of seawater salinity is further buried while chemically buffered by a different set of “Buffer 2” minerals. Buffer 2 includes the clay minerals Na-illite and K-illite in place of the albite and K-feldspar used in Buffer 1. The intensity of the alteration caused by burial past the initial chemical equilibration is very small as it was in the Buffer 1 case, but the mineralogic change is significantly different. For example, dolomite and Na-illite are precipitated rather than dissolved (compare Figure 29 to Figure 27).

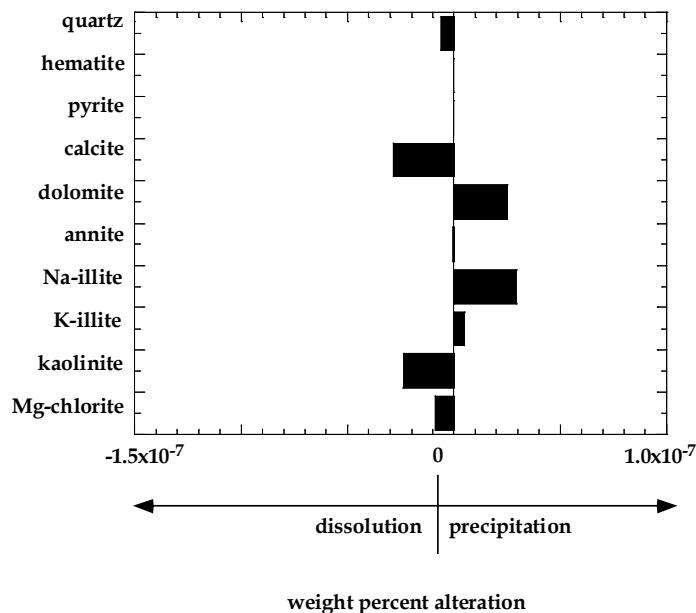


Figure 29: The weight percent mineral alteration due to the burial of saturated sediments from 2.75 to 3.0 km in equilibrium with Buffer 2 minerals (Table 8).

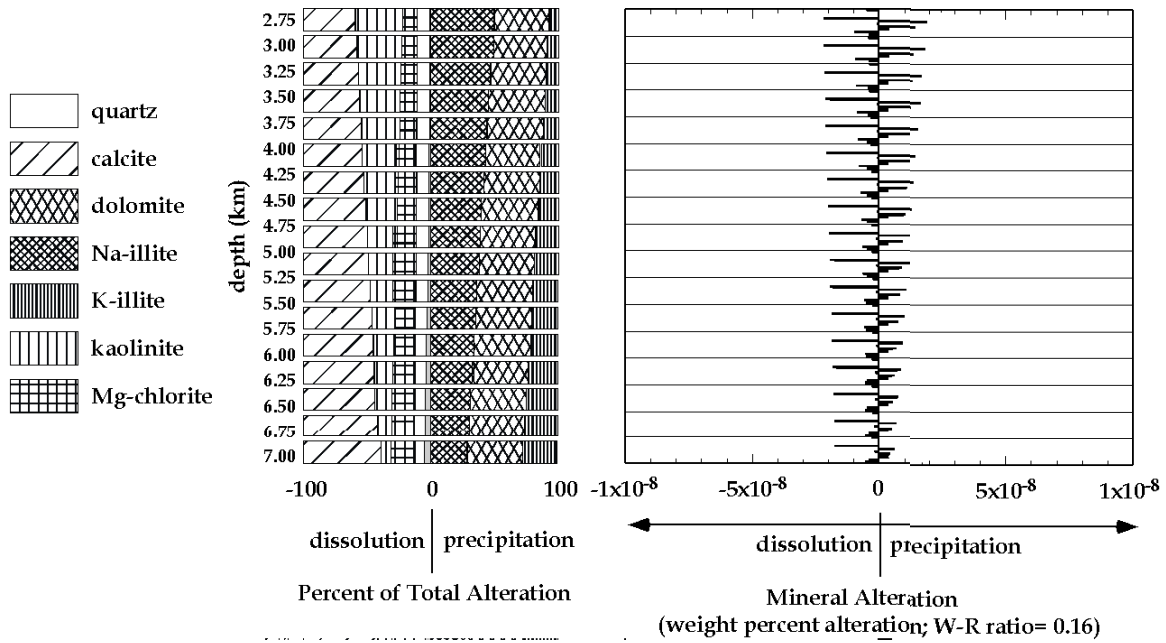


Figure 30: The percentage of minerals dissolved or precipitated, and the weight percent (of the total sediment mass) to successively greater depths due to continued sedimentation. Pore waters are always in equilibrium with Buffer 2 minerals (Table 8).

Table 8: The alteration that occurs as a sediment whose pore fluid is in equilibrium with the Buffer 2 mineral assemblage is moved from 2.75 to 3.00 km depth through the hydrostatic-normal geothermal 20°C/km) gradient shown in Figure 25.

	$g_{\text{alteration}} / g_{\text{rock}}$ per g_{water}	weight% (W/R=0.16)
quartz	-3.83×10^{-10}	-6.12×10^{-8}
hematite	9.56×10^{-14}	1.53×10^{-12}
pyrite	-3.68×10^{-14}	-5.89×10^{-13}
calcite	-1.77×10^{-9}	-2.83×10^{-8}
dolomite	1.56×10^{-9}	2.5×10^{-8}
annite	-2.65×10^{-11}	-4.24×10^{-10}
Na-illite	1.82×10^{-9}	2.92×10^{-8}
K-illite	3.20×10^{-10}	5.11×10^{-9}
kaolinite	-1.48×10^{-9}	-2.37×10^{-8}
Mg-chlorite	-5.44×10^{-10}	-8.7×10^{-9}

3. Flow Alteration in the Hydrostatic Zone

Sediments will be altered as fluids flow through them. As sediments are buried, their porosity decreases linearly from ~40% at the surface to ~10% at 5 km depth (Hunt et al., 1998). Fluid is released from the sediments as they compact, and this fluid moves through the basin. For the linear compaction profile just described, the expelled fluid crossing a surface as it is buried from 2 km to 4 km depth is ~30 kg/cm². An additional fluid volume of about the same magnitude is expelled as a result of organic maturation reactions with positive volume change. The flux through the sediments will, of course, not be uniform. Some areas (near faults, on the disturbed margins of salt domes, or at topographic highs in the top of overpressure) may receive much more throughput by attracting flow from other areas. The average discharge through the 3 km horizon should be ~60 kg/cm², but the discharge is likely to be very uneven. With these comments in mind, we will adopt a vertical flux of 200 kg cm⁻² as a “base case” reference for our alteration calculations. It is a reasonable estimate of the flow that should occur in areas where the expulsion of pore waters is slightly focused. The cumulative flux could be much greater if the focusing is greater than the factor of ~3 assumed here.

Table 9 and Figure 31 show the mineral alteration at 3 km depth caused by the upward vertical flow of 200 kg cm⁻² of pore water in the hydrostatic zone where the temperature gradient is 20°C km⁻¹ and the pressure 100 bars/km. The total dolomite precipitated is ~0.079 wt% of the sediment mass for the Buffer 1 calculation. For Buffer 2, dolomite dissolves at 3 km depth, but the total calcite precipitated is ~0.045 wt%.

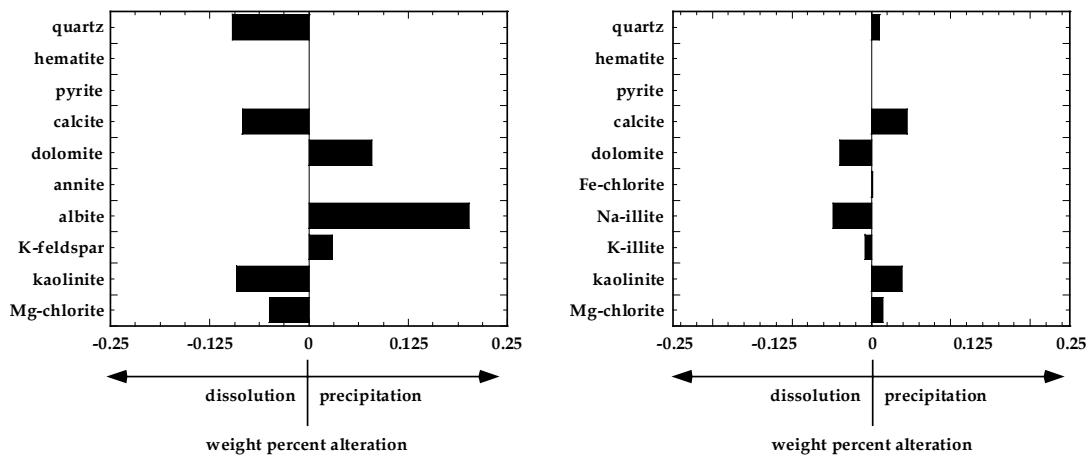


Figure 31: The weight percent mineral alteration of sediments at 3 km depth due to the vertical passage of 200 kg/cm² of pore fluid in equilibrium with Buffer 1 minerals (Table 3). Flow is in the hydrostatic zone (100 bars/km, 20°C/km) at ~3 km depth (see Figure 25).

Table 9: The mineral alteration caused by the vertical fluid flow of 200 kg/cm² pore water in equilibrium with a Buffer 1 (Table 3) and Buffer 2 (Table 8) mineral assemblage at ~3km depth. (+) denotes precipitation; (-) denotes dissolution.

	$\frac{\text{g alteration}}{\text{g rock}}$ per g _{water}		weight % (flux=2x10 ⁵)	$\frac{\text{g alteration}}{\text{g rock}}$ per g _{water}		weight % (flux=2x10 ⁵)
	Buffer 1			Buffer 2		
quartz	-4.79x10 ⁻⁹	-0.096		quartz	+4.92x10 ⁻¹⁰	0.010
hematite	-1.19x10 ⁻¹⁴	0.000		hematite	-9.89x10 ⁻¹⁴	0.000
pyrite	+4.68x10 ⁻¹⁴	0.000		pyrite	+3.88x10 ⁻¹⁴	0.000
calcite	-4.22x10 ⁻⁹	-0.084		calcite	+2.24x10 ⁻⁹	0.045
dolomite	+3.96x10 ⁻⁹	0.079		dolomite	-1.99x10 ⁻⁹	-0.040
annite	+4.98x10 ⁻¹³	0.000		Fe-chlorite	+3.08x10 ⁻¹¹	0.001
albite	+1.01x10 ⁻⁸	0.202		Na-illite	-2.38x10 ⁻⁹	-0.048
K-feldspar	+1.44x10 ⁻⁹	0.029		K-illite	-3.94x10 ⁻¹⁰	-0.008
kaolinite	-4.54x10 ⁻⁹	-0.091		kaolinite	+1.93x10 ⁻⁹	0.039
Mg-chlorite	-2.52x10 ⁻⁹	-0.050		Mg-chlorite	+6.83x10 ⁻¹⁰	0.014

4. Alteration Due to Flow through Pressure Seals

The nature of the pressure gradient within the pressure transition zone is a matter of current debate. Many investigators believe that the pressure transition zone is a low-permeability massive shale. Another possibility is that gas capillary sealing is responsible for seal integrity. A difference between these two sealing concepts that we can address here is the nature of the chemical alteration that occurs in distinctly different pressure profiles of these two seals.

Consider the top 40 meters (2.995 to 3.035 km) of a pressure transition zone (Figure 32). The uppermost 5 meters of this section is in the hydrostatic zone ($\partial P / \partial z = 100 \text{ bar km}^{-1}$) above the pressure transition and has a temperature gradient, $\partial T / \partial z$, of 20°C km^{-1} . The next 35 meters (3,000 to 3,035 km) lie within the pressure transition zone.

In the massive shale (lithologic seal) case, overpressure is caused by low sediment permeability and the pressure gradient is uniform. In this seal, $\partial P / \partial z = 500 \text{ bar/km}$ and $\partial T / \partial z = 2500 \text{ bars/km}$. In each 5 m depth increment, pressure increases by 2.5 bars and temperature by 0.25°C . This is shown in Figure 32a.

Figure 32b illustrates the upper 30 m of the pressure transition zone for the “capillary seal” case. Here the pressure profile is “stepped” with pressure drops of 12.5 bars ($\partial P / \partial z = 2500 \text{ bars/km}$) occurring across 5 m intervals spaced 20 m apart. The pressure gradient is 0 bars/km in the 20 m intervals. The temperature gradient is 50°C/km in both the steep and zero-pressure gradient intervals.

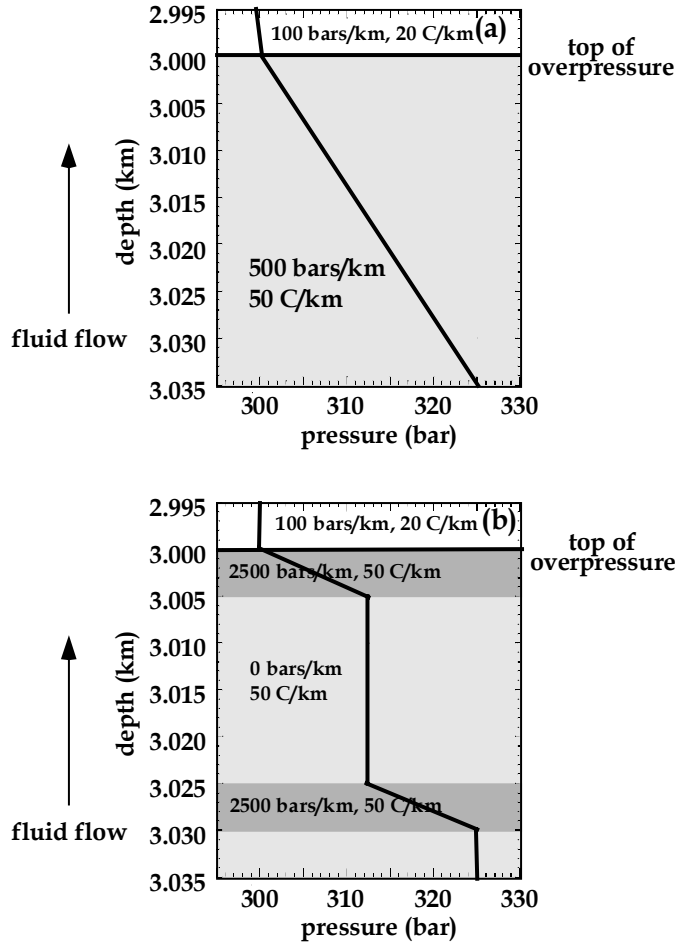


Figure 32: The pressure gradients used in calculating mineral alteration through the top 35 meters of a pressure transition zone. (A) A linear pressure gradient through a lithostatic seal. (B) A stepped pressure gradient through a capillary seal where the pressure drop occurs entirely across two thin layers within the seal where there is gas capillary blockage. The pressure transition zone is shaded with darker shading indicating steeper pressure gradients.

As a prelude to looking at the mineral alteration due to fluid flow through a seal, we calculate the alteration for hydrostatic ($\partial P / \partial z = 100 \text{ bar km}^{-1}$) conditions with a normal temperature gradient $\partial T / \partial z = 20^\circ\text{C km}^{-1}$. The results for the interval 2.995-3.010 km are shown in Figure 33. The intensity of alteration is identical to that shown in Figure 31, but the plot style is identical to the seal alteration plots that follow. The total weight percent of minerals precipitated for Buffer 1 is ~ 0.30 ; for Buffer 2 it is $\sim 0.05 \text{ wt\%}$.

Figure 34 shows that the alteration in a lithologic (Figure 32a) seal is the same (for both buffers) but is 3 times more intense. Figure 35 shows that the alteration is constant with depth.

Figure 36 shows that the alteration in the steep pressure gradient intervals of the capillary (Figure 32b) seal is nine times greater than in the hydrostatic zone above the seal and three times greater than in the constant pressure intervals of the seal. Figure 37 shows the

pattern of alteration does not change significantly with depth for either buffer. A feature of interest is the fact that the alteration in the steep pressure gradient intervals is the same as in the zero-gradient intervals for Buffer 1 but not for Buffer 2. This is shown most clearly in the percent mineral alteration diagrams of Figures 38 and 39.

No Seal Case

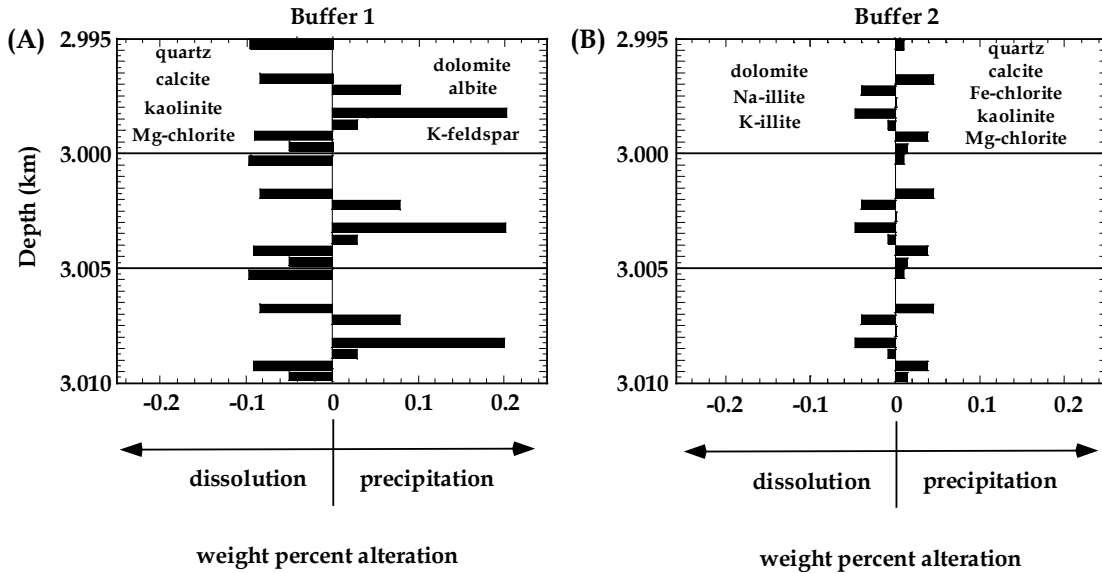


Figure 33: The weight percent (of the sediment mass) mineral alteration caused by the vertical flow of 200 kg/cm² of pore water in equilibrium with Buffer 1 and Buffer 2 minerals (Tables 3 and 8) at ~3 km depth in the hydrostatic zone (100 bars/km, 20°C/km; Figure 25).

Lithologic Seal Case

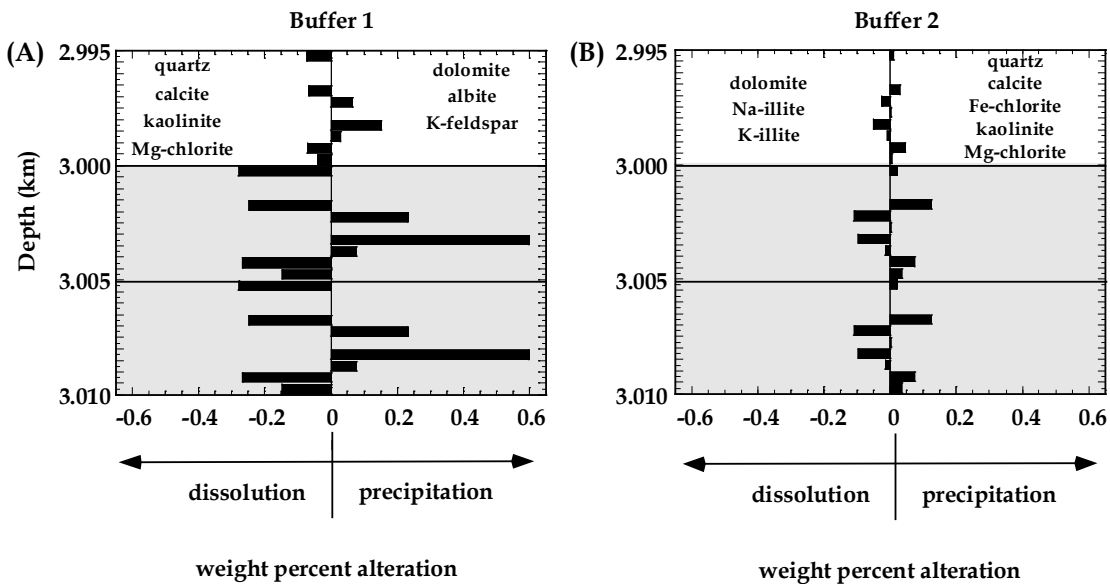


Figure 34: The weight percent mineral alteration caused by the vertical flow of 200 kg/cm² pore fluids in equilibrium with Buffer 1 and Buffer 2 minerals (Tables 3 and 8) through a lithostatic seal ($dT/dz=50C/km$ and $dP/dz=500$ bar/km; Figure 25) and the overlying hydrostatic zone (not shaded, $dT/dz=20C/km$ and $dP/dz=100$ bar/km).

Lithostatic Seal Case

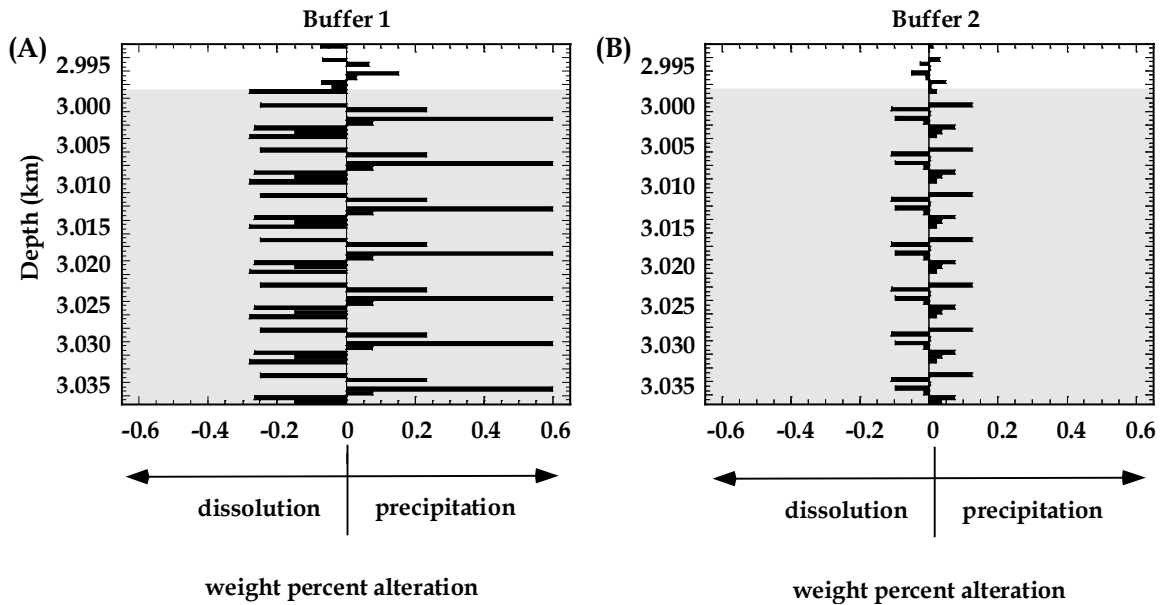


Figure 35: The weight percent mineral alteration caused by the vertical flow of 200 kg/cm² pore fluid through an expanded interval of lithologic seal (shaded zone, dT/dz=50C/km; dP/dz=500 bar/km) and a portion of the overlying hydrostatic zone (unshaded, dT/dz=20C/km, dP/dz=100 bar/km).

Capillary Seal Case

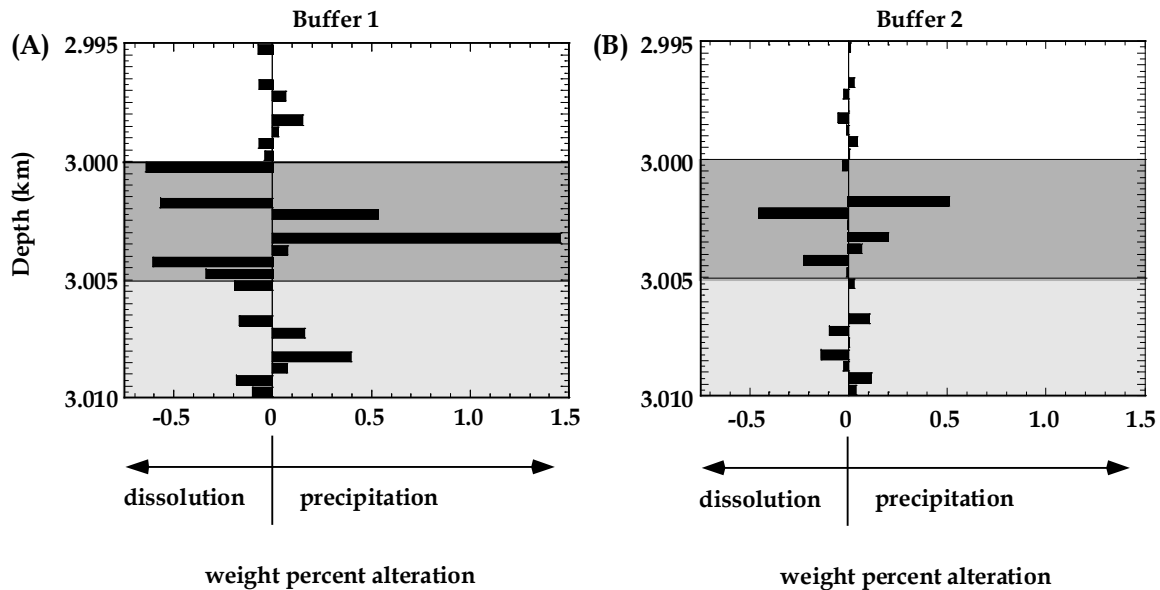


Figure 36: The weight percent mineral alteration caused by the vertical flow of 200 kg/cm² through a capillary seal and parts of the overlying hydrostatic zone (see Figure 32) in equilibrium with Buffer 1 and Buffer 2 minerals (Tables 3 and 8). The hydrostatic zone is unshaded and dT/dz=20C/km, dP/dz=200 bar/km. In the 250 dark shaded region dT/dz=50C/km, dP/dz=2500 bar/km; in the light shaded region dT/dz=50C/km, dP/dz=0 bar/km.

Capillary Seal Case

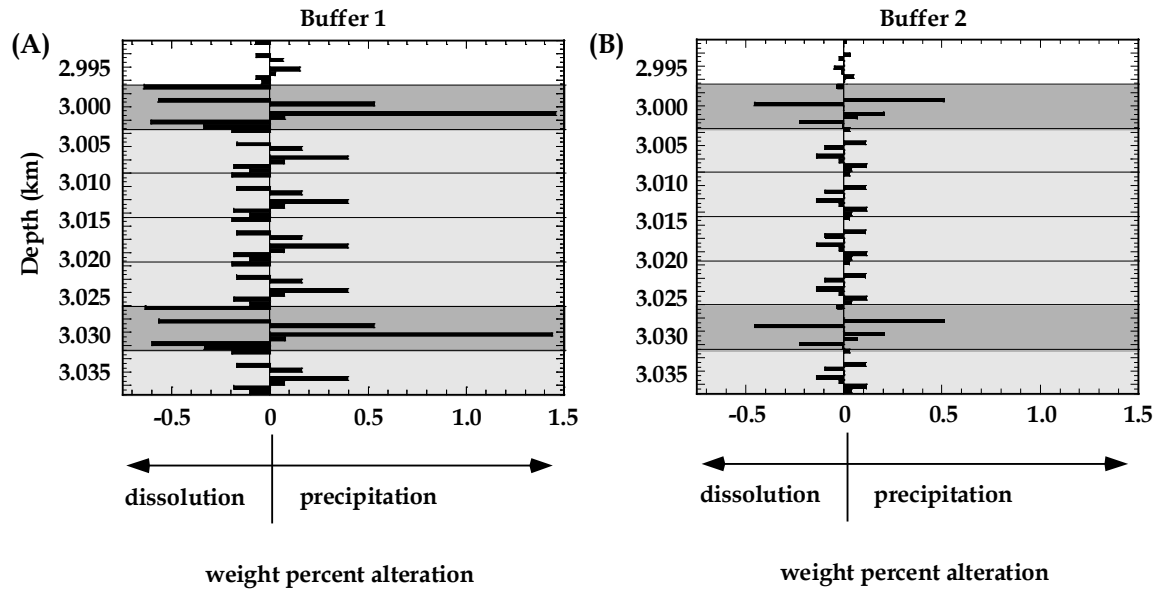


Figure 37: The weight percent mineral alteration caused by the vertical flow of 200 kg/cm^2 pore fluids in a capillary seal in equilibrium with Buffer 1 and Buffer 2 minerals (Tables 3 and 8). Shading convention is the same as in Figure 36.

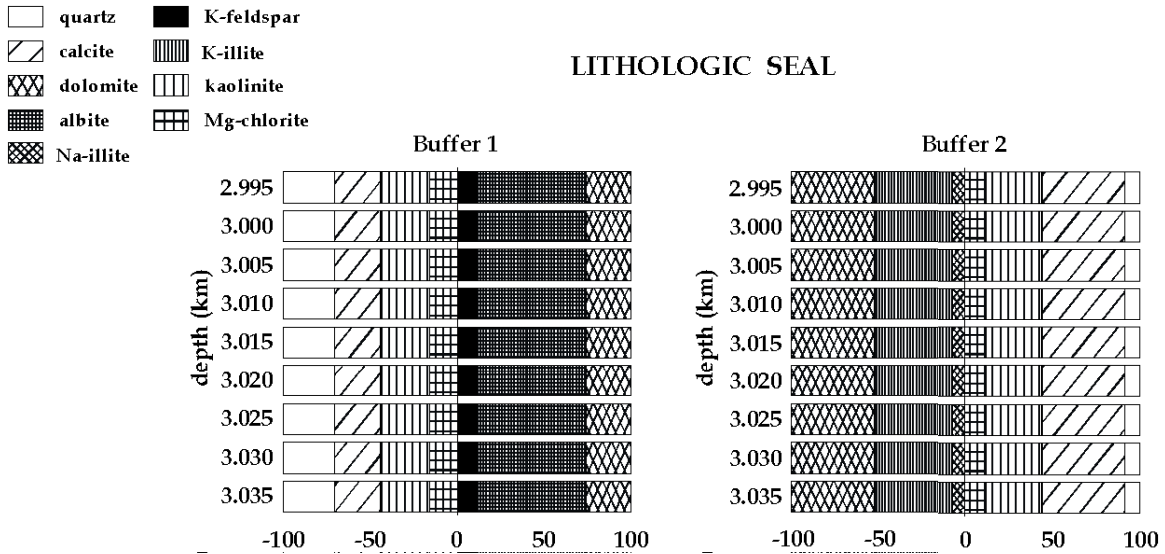


Figure 38: The percentages of minerals dissolved and precipitated due to fluid flow upward through the lithologic seal whose weight percent alteration is shown in Figure 35.

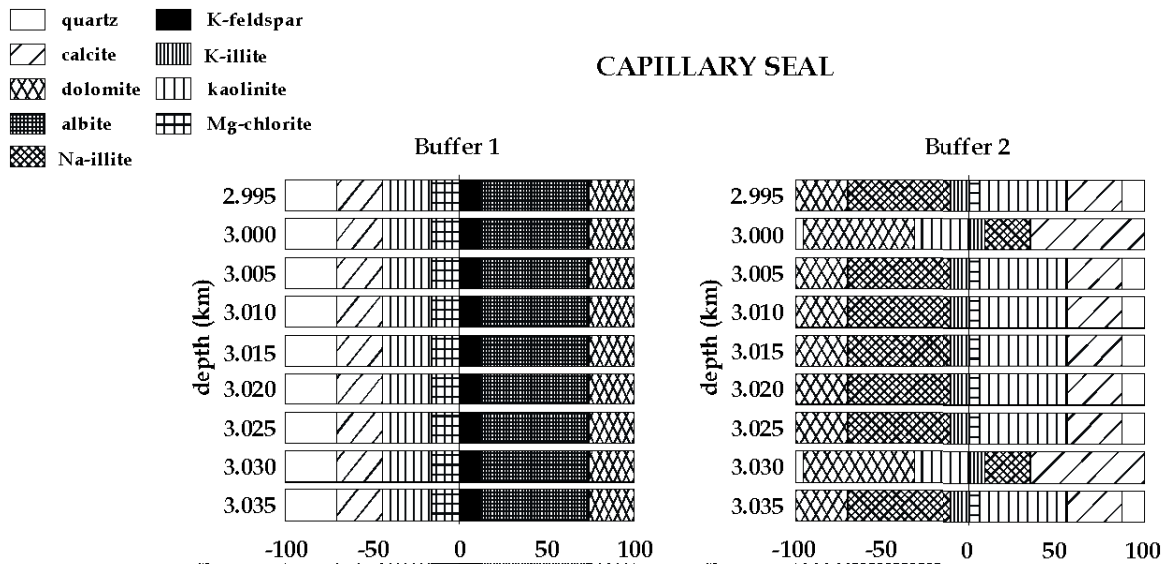


Figure 39: The percentages of minerals dissolved and precipitated due to fluid flow upward through the capillary seal whose weight percent alteration is shown in Figure 37.

5. Inorganic Alteration as a Function of Gas Saturation

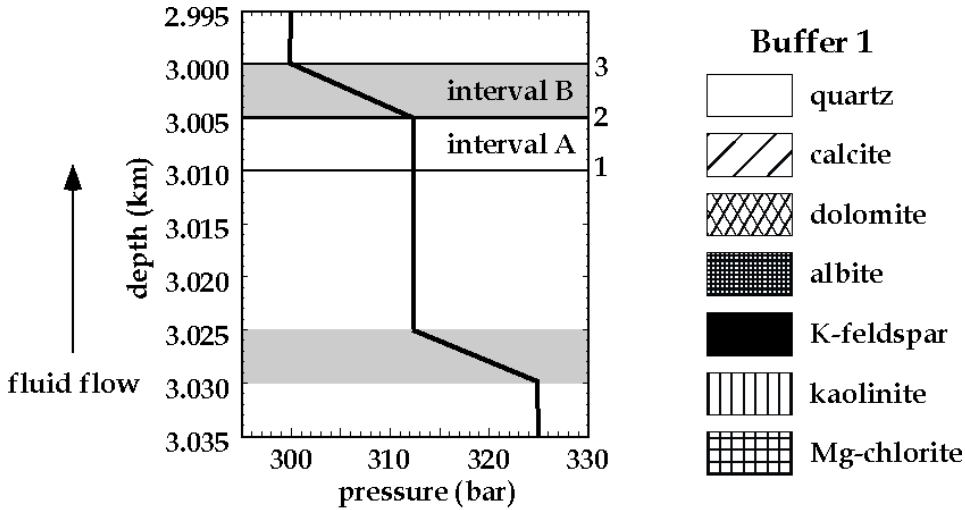
The previous cases have not taken into account the chemical consequences of the presence of gas in the sediment pores. Gas is often present as a pore fluid and can act as a capillary sealing agent in sedimentary basins. The mineralogical alteration of sediment in the presence of a gas phase is modified because volatile chemical species fractionate into and are transported in the gas phase. This modified advection of the basis species drives a different mineralogical change. Gas is of particular interest within the pressure transition of the capillary seal (Figure 32b), so we limit our discussion in this case.

We calculate the effects of gas flow by specifying the mass fraction of gas in the total fluid flux (γ in equation (4)). Figure 40 illustrates the effects of gas transport on mineralogical change for Buffer 1, a temperature gradient of $50^{\circ}\text{C km}^{-1}$, and a constant pressure of 312.5 bars. When the pore fluid is single phase (0% gas flux), the minerals precipitating are dolomite, albite, and K-feldspar. As the fraction of gas flux increases, the proportions of albite and K-feldspar precipitation decrease. At ~60% gas saturation, kaolinite begins to precipitate.

Figure 41 shows that the alteration is quite different in zones where the pressure gradient is steep. At 0% gas flux, the alteration is essentially the same as in the interval over which pressure remains constant, but as the gas flux increases less dolomite precipitates. Above ~60% gas saturation, dolomite dissolves, and Mg-chlorite and calcite precipitate instead. This is very different from the adjacent constant-pressure interval (Figure 40).

Figures 42 and 43 show the same calculations for Buffer 2. The character of alteration is different in the steep and zero pressure gradient zones, but the changes with gas fraction are not as dramatic.

Capillary Seal, Interval A, Buffer 1



Interval A: $P_2=312.5$ bar; $T_2=80.25$ C
 $P_1=312.5$ bar; $T_1=80.50$ C

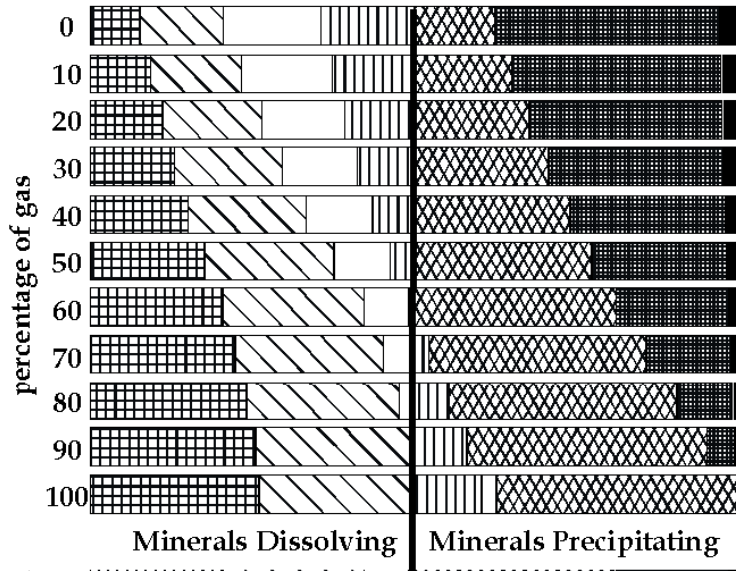
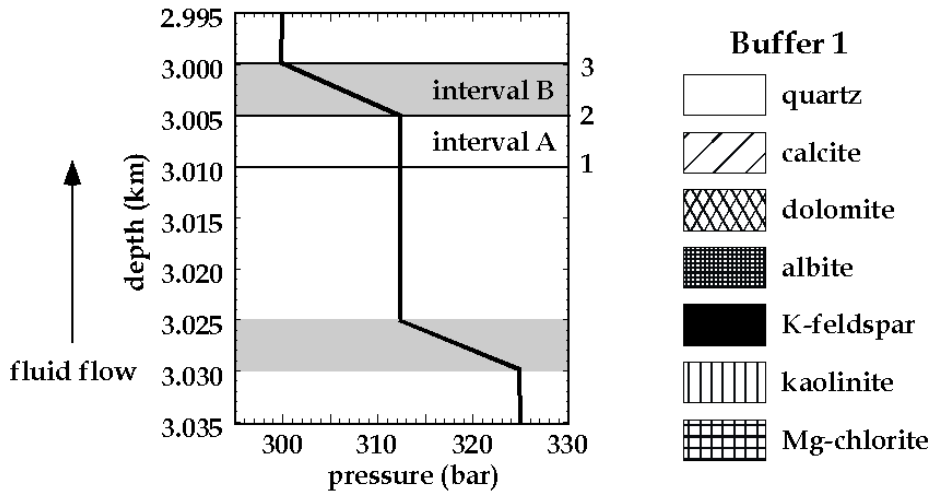


Figure 40: Mineralogic change as a function of the percent of the total fluid flux that is gas in "interval A" of a capillary seal. The total vertical mass flux is 200 kg/cm². Interval A has a temperature gradient of 50C/km and a constant pressure of 312.5 bars. Shading in the top figure indicates the steep pressure gradient intervals.

Capillary Seal, Interval B, Buffer 1



Interval B: $P_2=300.0$ bar; $T_2=80.00$ C
 $P_1=312.5$ bar; $T_1=80.25$ C

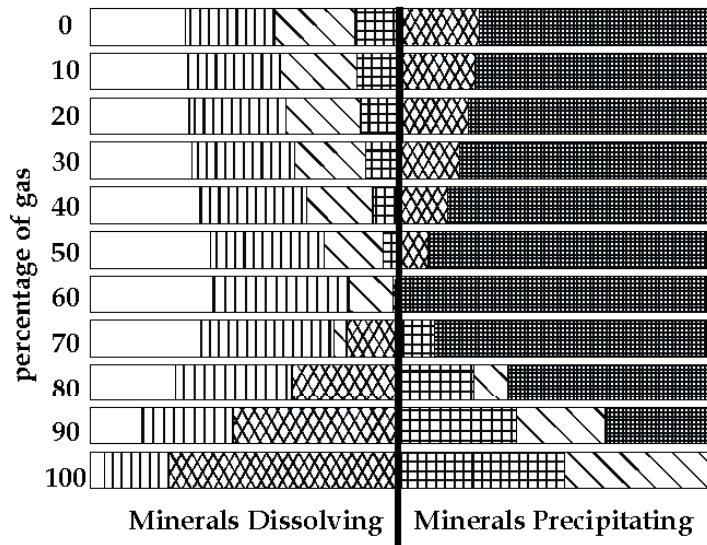
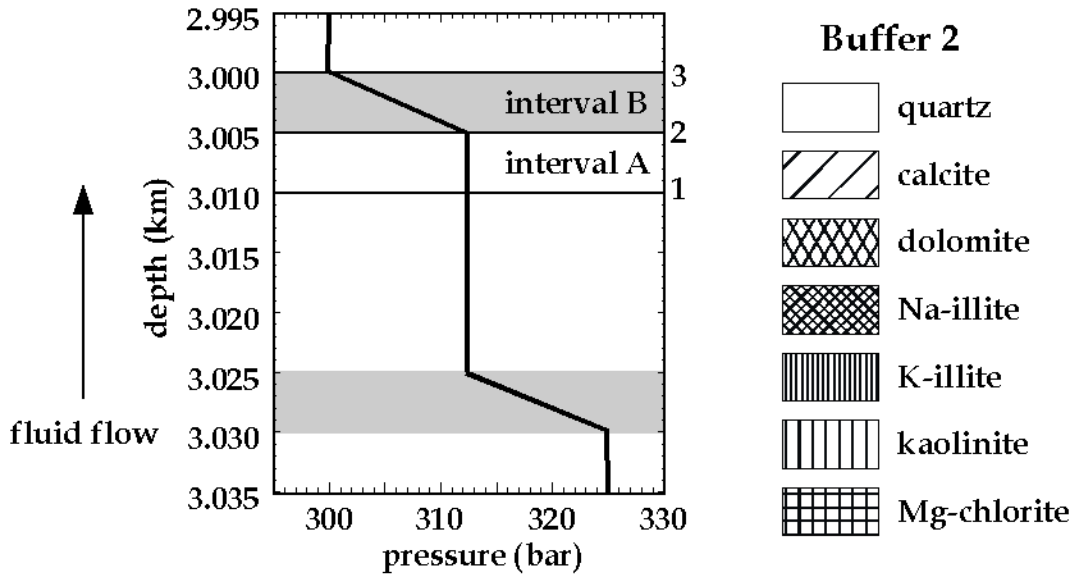


Figure 41: Mineralogic change as a function of the percent of the total fluid flux that is gas in “interval B” of a capillary seal. The total vertical mass flux is 200 kg/cm². Interval B has a temperature gradient of 50°C/km and a pressure gradient of 2500 bars/km. Shading in the top figure indicates the steep pressure gradient intervals.

Capillary Seal, Interval A, Buffer 2



Interval A: $P_2=312.5$ bar; $T_2=80.25$ C

$P_1=312.5$ bar; $T_1=80.50$ C

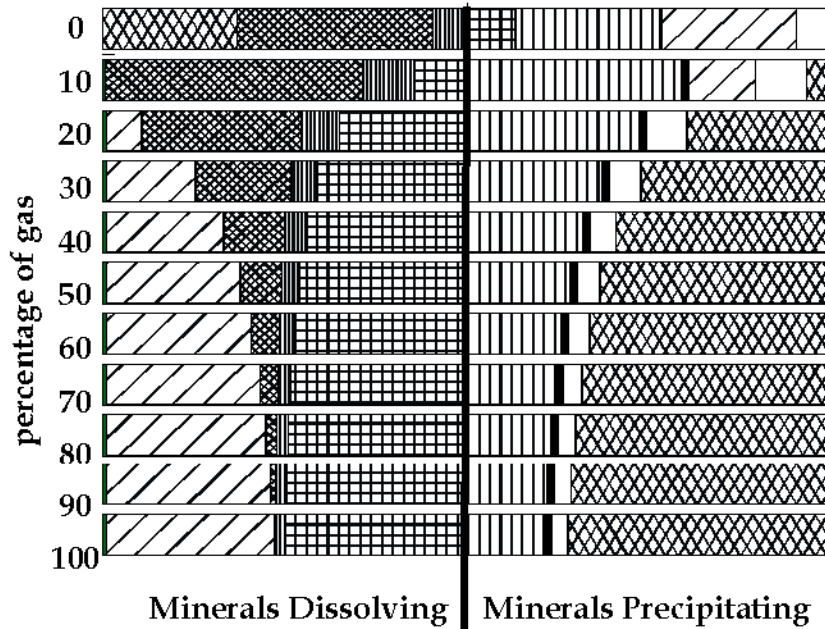
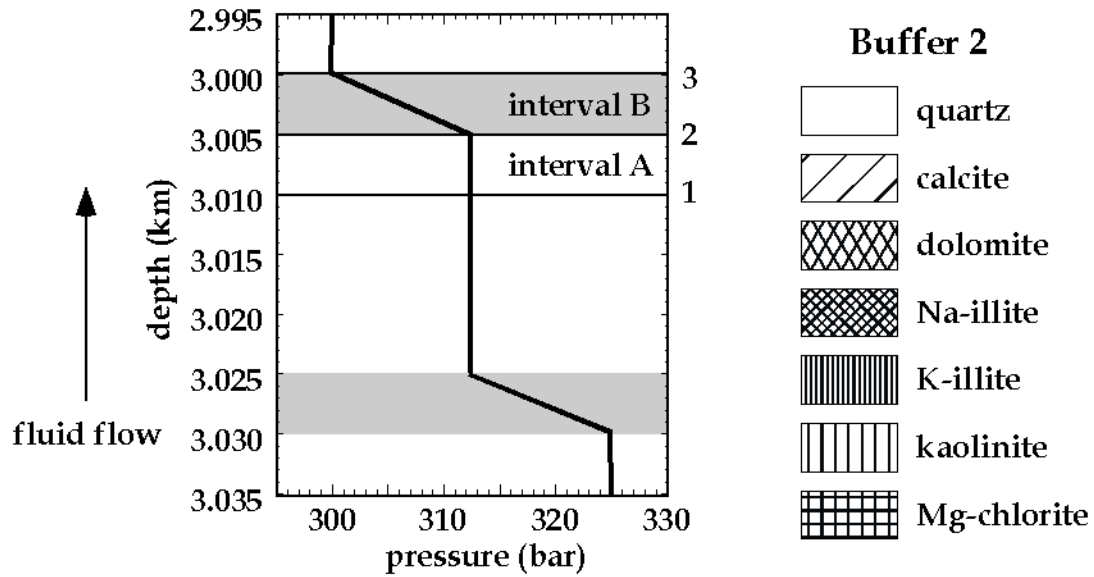


Figure 42: Mineralogic change as a function of the percent of the total fluid flux that is gas in “interval A” of a capillary seal. The total vertical mass flux is 200 kg/cm². Interval A has a temperature gradient of 50°C/km and a constant pressure of 312.5 bars. Shading in the top figure indicates the steep pressure gradient intervals.

Capillary Seal, Interval B, Buffer 2



Interval B: $P_2=300.0$ bar; $T_2=80.00$ C
 $P_1=312.5$ bar; $T_1=80.25$ C

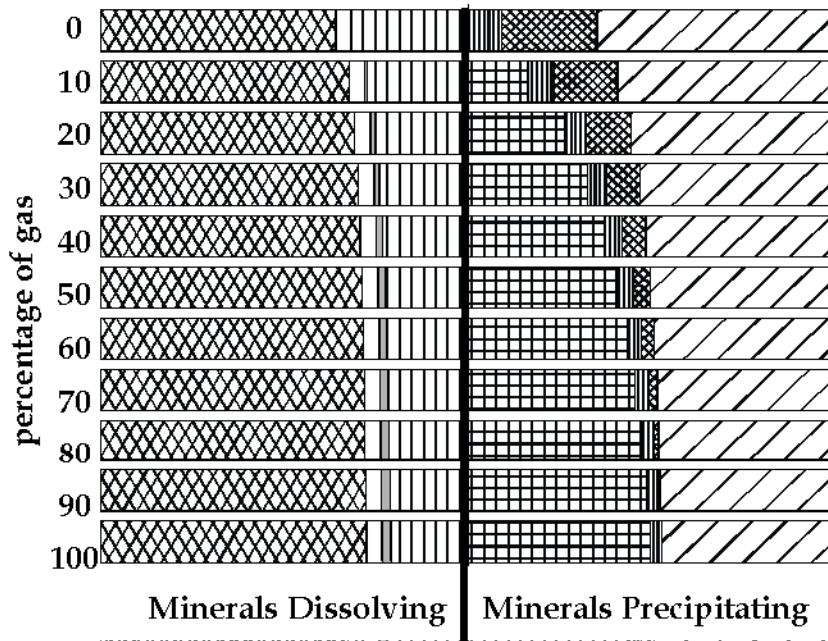


Figure 43: Mineralogic change as a function of the percent of the total fluid flux that is gas in “interval B” of a capillary seal. The total vertical mass flux is 200 kg/cm^2 . Interval B has a temperature gradient of 50°C/km and a pressure gradient of 2500 bars/km . Shading in the top figure indicates the steep pressure gradient intervals.

6. Inorganic Alteration as a Function of Salinity

In all of the previous cases, the salinity has been assumed equal to that of seawater (0.5 molal $[Cl^-]$). Increasing in salinity increases the intensity of alteration. Inorganic alteration due to the upward movement of fluids through a pressure seal with a stepped pressure gradient at salinities equivalent to seawater ($m_{Cl^-} = 19,000$ ppm) and twice seawater ($m_{Cl^-} = 38,000$ ppm) are shown in Figure 44 for Buffer 1 and in Figure 45 for Buffer 2. The weight percent alteration increases by a factor of ~ 2.5 in the case of Buffer 1 and ~ 4 for Buffer 2 (note the change in scale on the horizontal weight percent axis).

Capillary Seal, Buffer 1

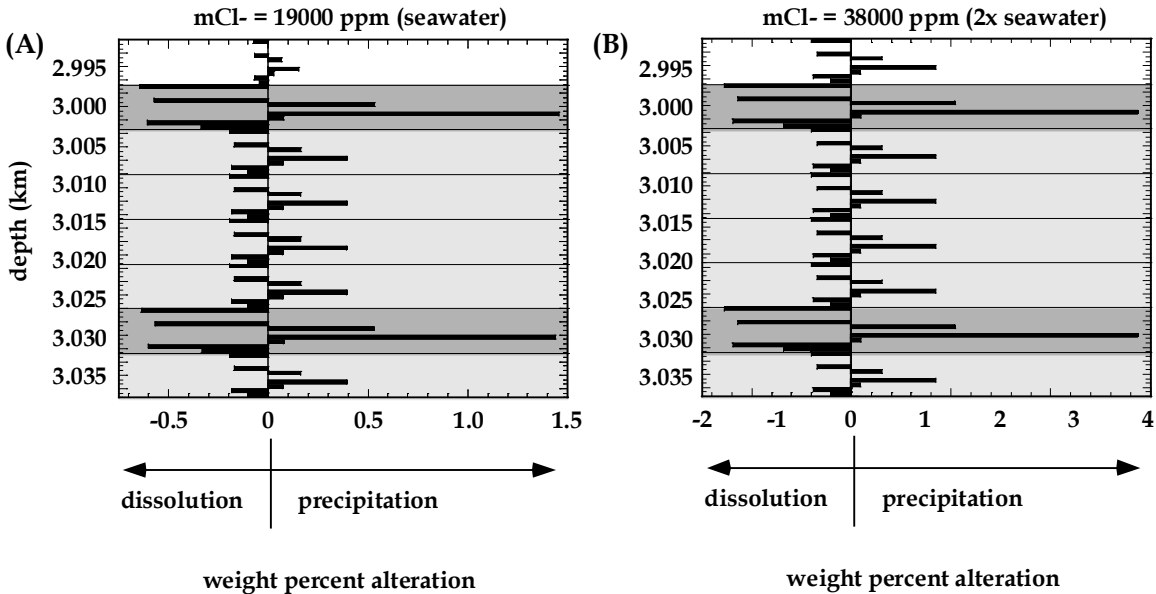


Figure 44: Doubling pore fluid salinity more than doubles alteration intensity. Vertical fluid flow is 200 kg/cm^2 through a capillary seal with fluids in equilibrium with Buffer 1 minerals (Table 3). Shading indicates pressure gradient: No shading, $dT/dz=20C/km$, $dP/dz=100$ bar/km, dark shade $dT/dz=50C/km$, $dP/dz=2500$ bar/km, lighter shading $dT/dz=50C/km$, $dP/dz=0$ bar/km. Fluid is in equilibrium with Buffer 1 (see Figure 5.18). Note weight percent scale of the two figures is different and 2x salinity case has much more intense alteration.

Capillary Seal, Buffer 2

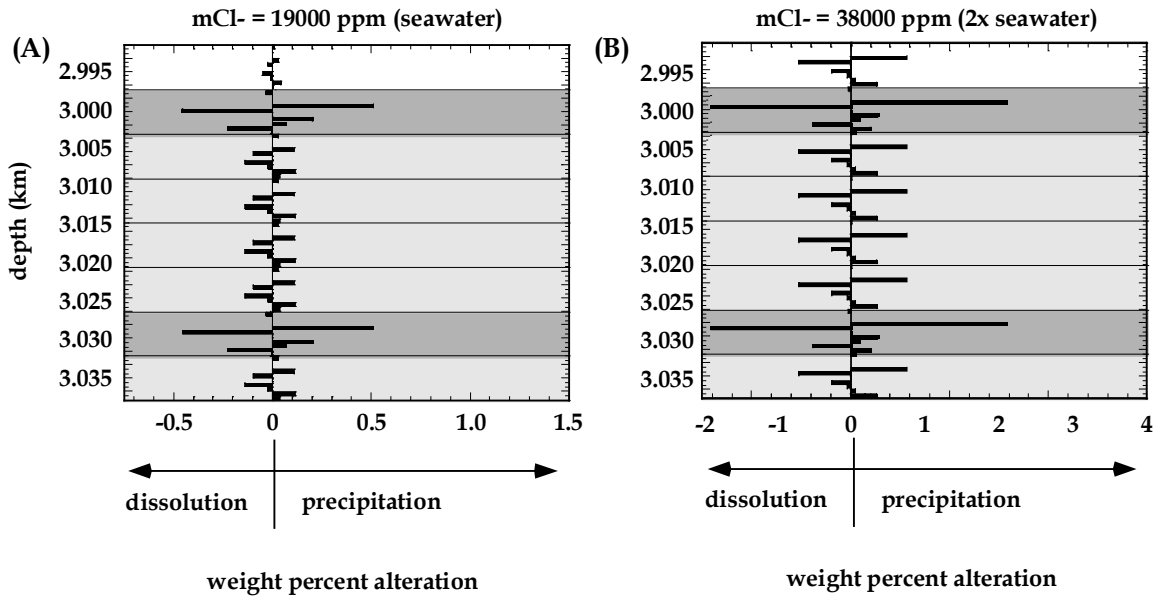


Figure 45: Doubling pore fluid salinity more than doubles alteration intensity. Vertical fluid flow is 200 kg/cm² through a capillary seal with fluids in equilibrium with Buffer 2 minerals (Table 8). Shading indicates pressure gradient: No shading, dT/dz=20C/km, dP/dz=100 bar/km, dark shade dT/dz=50C/km, dP/dz=2500 bar/km, lighter shading dT/dz=50C/km, dP/dz=0 bar/km.

7. Estimating the Cumulative Fluid Flux as a Function of Intensity of Alteration

For specified conditions we can determine the amount of fluid throughput from inorganic alteration. Figures 46 and 47 plot the log of the cumulative vertical fluid flux through sediments as a function of the intensity of mineralogical alteration (the sum of precipitated minerals). The different lines depict different temperature-pressure profiles and different percentages of gas. The cumulative flux is plotted for two salinities in each figure. Figure 46 is calculated for Buffer 1, Figure 47 is calculated for Buffer 2. The log alteration intensity increases linearly with the log fluid flux for all situations. The alteration in the steep pressure gradient portions of the capillary seal is the most intense. The fluid is 0% gas unless otherwise indicated.

The plots can be used to determine the fluid flux through sediments from the total observed weight percent of authigenic mineral abundance. Suppose for example that the weight percent of authigenic (new alteration minerals) is 1.0%. In order to explain 1 wt% alteration due to the passage of a fluid in equilibrium with Buffer 1 we would need a cumulative flux of 650 kg of fluid per cm² (area perpendicular to flow or plan if flow is vertical as here) seawater salinity pore waters (0.5 mol L⁻¹ [Cl⁻]) in a hydrostatic-geothermal ($\partial P / \partial z = 100 \text{ bar km}^{-1}$, $\partial T / \partial z = 20^\circ\text{C km}^{-1}$) setting. In a lithologic seal ($\partial P / \partial z = 500 \text{ bar km}^{-1}$, $\partial T / \partial z = 50^\circ\text{C km}^{-1}$), 250 kg/cm² fluid throughput is required to produce the 1 wt% alteration. In the high pressure gradient parts of a capillary seal

($\partial P / \partial z = 2,500 \text{ bar km}^{-1}$, $\partial T / \partial z = 50^\circ\text{C km}^{-1}$), 130 kg/cm^2 would be required (250 kg/cm^2 if the fluid is 50% gas).

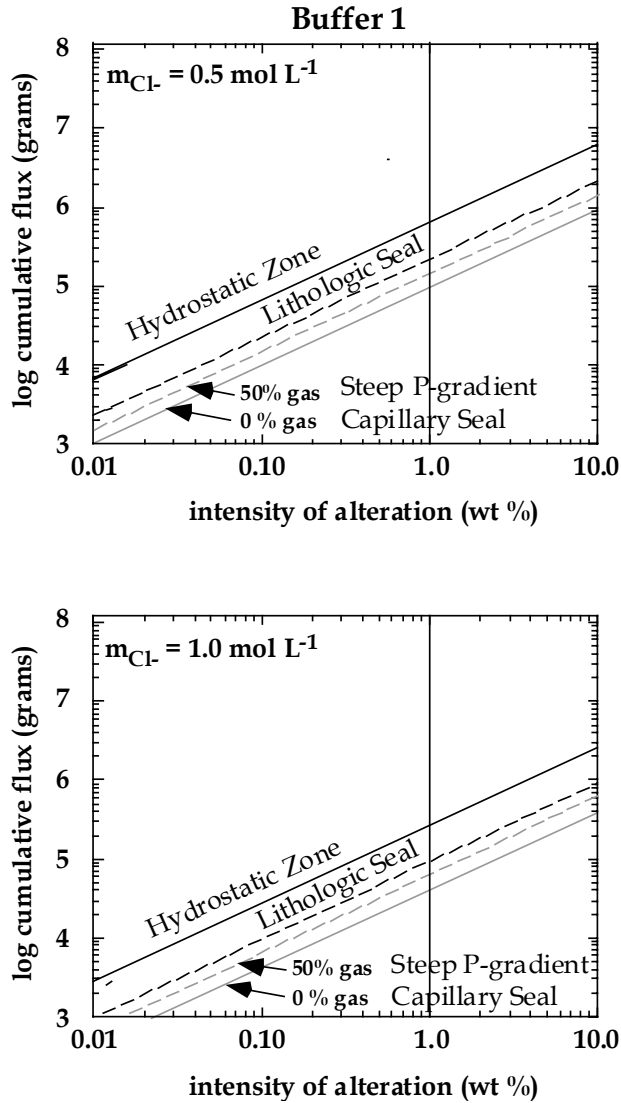


Figure 46: The log of the cumulative flux through sediments as a function of the intensity of total Buffer 1 alteration. Vertical line at 1% alteration shows approximate intensity of minimum expected flow-related alteration.

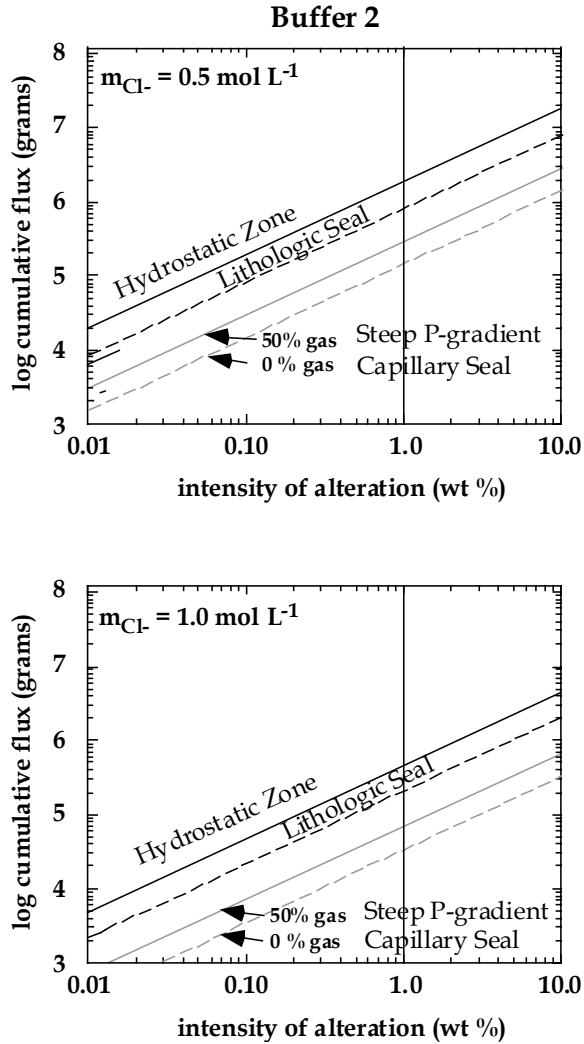


Figure 47: The log of the cumulative flux through sediments as a function of the intensity of total Buffer 2 alteration. Vertical line at 1% alteration shows approximate intensity of diagenetic alteration.

For Buffer 2 we would need a cumulative flux of $1,900 \text{ kg/cm}^2$ of seawater salinity fluid through a hydrostatic-geothermal pressure gradient, of 850 kg/cm^2 through a lithologic seal, and 100 kg/cm^2 through the steep pressure gradient portion of a lithologic seal (300 kg/cm^2 if 50% gas is present).

The required fluid throughput is reduced by a factor of ~ 3 if the salinity of the pore waters is twice seawater salinity rather than seawater salinity.

The character of alteration can, in principle, distinguish between the various possible pressure and temperature gradients. For example, Na- or K-illite are only precipitated in the steep pressure gradient parts of the capillary seal. If these minerals are present, a 1% alteration would indicate a cumulative fluid flux of between 100 and 300 kg/cm^2 depending on the fraction of gas.

8. Discussion

A primary goal of the work reported here was to evaluate the prospect of using inorganic alteration as a flow meter to assess the amount of fluid that has moved through sedimentary basin seals. We have shown how seal alteration can be calculated and how the fluid throughput can be estimated from petrographic measurements of alteration. The alteration expected from fluid flow through seals is significant. It is ten times greater than a minimum estimate of diagenetic alteration for minor focusing of brine discharge. The intensity of alteration depends on many factors. Some of the factors can be eliminated. For example, petrographic observations will directly indicate the mineral buffer that should be used in calculations. Present-day pore water salinities in the altered interval may give some guidance regarding the fluid salinities that are most appropriate. Alteration mineralogy may indicate very steep pressure gradients and suggest a capillary seal. Even without these constraints useful estimates can be made from Figures 46 and 47. Ultimately, the complexity of the mineralogic alteration could provide an advantage. Clearly alteration mineralogy contains a lot of potentially valuable information regarding basin processes and the nature of sealing. This report provides a theoretical basis for extracting this information from seal alteration.

The main barrier to application of the methods developed here is mapping of the alteration intensity in a basin. The most useful way to do this is by seismic interval velocity analysis because this could provide a synoptic view of alteration that could be converted to fluid flux maps. The alteration we calculate is intense enough that it should impact seismic wave velocities, particularly where flow is focused. We know that alteration could be seismically mapped in particular horizons. Hopefully the theoretical work presented here and the promise of converting alteration for flow maps will stimulate others to investigate seriously whether seismic techniques could be used to map alteration in sedimentary basins.

G. Acknowledgments

The work reported here is abstracted from the Ph.D. thesis of J. D. Shosa. The thesis drew on earlier work by L. M. Cathles. The authors would like to thank GRI for supporting Shosa through her entire graduate career. We would like to especially thank Richard Parker, our GRI contract manager for his steady support and encouragement.

H. References

- Cathles, L. M., 1991, The importance of vein salvaging in controlling the intensity and character of subsurface alteration in hydrothermal systems: *Economic Geology*, v. 86, pp. 466-471.
- Cathles, L. M., and Shea, M. E., 1992, Near-field high temperature transport: evidence from the genesis of the Osamu Utsumi uranium mine, Poços de caldeas alkaline complex, Brazil: *Journal of Geochemical Exploration*, v. 45, pp. 565-603.
- Cathles, L. M., 2001, Capillary seals as a cause of pressure compartmentation in sedimentary basins: *Petroleum Systems of Deep-Water Basins: Global and Gulf of Mexico Experience*, Houston, Texas, GCSSEPM, pp. 561-571.

- Chermak, J. A., and Rimstidt, J. D., 1989, Estimating the thermodynamic properties (ΔG_f° and ΔH_f°) of silicate minerals from the sum of polyhedral contributions: *American Mineralogist*, v. 74, pp. 1023-1031.
- Ellis, A. J., 1970, Quantitative interpretation of chemical characteristics of hydrothermal systems: *Geothermics*, Special Issue 2, pt. 1, pp. 516-528.
- Erendi, A., and Cathles, L. M., 2001, Gas capillary inhibition to oil production: *Petroleum Systems of Deep-Water Basins: Global and Gulf of Mexico Experience*, Houston, Texas, GCSSEPM, pp. 607-618.
- Fei, Y., and Saxena, S. K., 1987, An equation of state for the heat capacity of solids: *Geochimica et Cosmochimica Acta*, v. 51, pp. 251-254.
- Hanor, J. S., 1994, Physical and chemical controls on the composition of waters in sedimentary basins: *Marine and Petroleum Geology*, v. 11, no. 1.
- Hazen, R. M., 1988, A useful fiction: Polyhedral modeling of mineral properties: *American Journal of Science*, v. 288-A, pp. 242-269.
- Helgeson, H. C., and Kirkham, D. H., 1974, Theoretical prediction of the thermodynamic behavior of aqueous electrolytes at high pressures and temperatures: I. Summary of the thermodynamic/electrostatic properties of the solvent: *American Journal of Science*, v. 274, pp. 1089-1198.
- Helgeson, H. C., and Kirkham, D. H., 1976, Theoretical prediction of the thermodynamic behavior of aqueous electrolytes at high pressures and temperatures: III. Equations of state for aqueous species at infinite dilution: *American Journal of Science*: v. 276, pp. 97-240.
- Huang, W. H., and Keller, W. D., 1973, Gibbs free energies of formation calculated from dissolution data using specific mineral analyses: III. Clay minerals: *American Mineralogist*, v. 58, pp. 1023-1028.
- Johnson, J. W., Oelkers, E. H., and Helgeson, H. C., 1992, SUPCRT92: Software package for calculating the standard molal thermodynamic properties of minerals, gases, aqueous species, and reactions from 1 to 5000 bars and 0° to 1000°C: *Computers in Geoscience*, v. 18, pp. 899-947.
- Klein, C., and Hurlbut, C. S., 1985, *Manual of Mineralogy*, John Wiley & Sons. New York, NY, 596 pp.
- Maier, C. G., and Kelley, K. K., 1932, An equation for the representation of high-temperature heat content data: *American Chemical Society Journal*, v. 54, pp. 3242-3246.
- Meulbroek, P., 1997, Hydrocarbon phase fractionation in sedimentary basins, Ph.D. thesis, Cornell University, Ithaca, NY, 345 pp.
- Meulbroek, P., 1998, Phase fractionation at South Eugene Island Block 330: *Organic Geochemistry*, v. 29, pp. 223-229.
- Nordstrum, D. K., and Munoz, J. L., 1985, *Geochemical Thermodynamics*, Benjamin/Cummings Publishing Company, Inc., Menlo Park, CA.
- Reed, M. H., and Spycher, N. F., 1985, Boiling, cooling, and oxidation in epithermal systems: A numerical modeling approach, in Berger, B. R., and Bethke, P. M.

- (editors), *Reviews in Economic Geology Volume 2: Geology and Geochemistry of Epithermal Systems*, SEPM, pp. 249-272.
- Reesman, A. L. and Keller, W. D., 1967, Chemical composition of illite: *Journal of Sedimentary Petrology*, v. 37, pp.592-596.
- Revil, A., and Cathles, L. M., 2001, The porosity-depth pattern defined by 40 wells in Eugene Island South Addition, Block 330 Area, and its relation to pore pressure, fluid leakage, and seal migration: *Petroleum Systems of Deep-Water Basins: Global and Gulf of Mexico Experience*, Houston, Texas, GCSSEPM, pp. 687-712.
- Robinson, G. R., and Haas, J. L., 1983, Heat capacity, relative enthalpy, and calorimetric entropy of silicate minerals: An empirical method of prediction: *American Mineralogist*, v. 68, pp. 541-553.
- Ross, T. P., Rose, A. W., and Poulson, S. R., 1994, Pore fluid chemistry of a pressure transition zone, Moores-Sam-Morganza gas field, Tuscaloosa Trend, Louisiana, in Orteleva, P. J. (editor), *Basin Compartments and Seals: AAPG Memoir 66*, pp. 97-117.
- Shosa, J. D., 2000, Overpressure in sedimentary basins: Mechanisms and mineralogical implications, Ph.D. thesis, Cornell University, Ithaca, NY, 214 pp.
- Shosa, J. D., and Cathles, L. M., 2001, Experimental investigation of capillary blockage of two phase flow in layered porous media: *Petroleum Systems of Deep-Water Basins: Global and Gulf of Mexico Experience*, Houston, Texas, GCSSEPM, pp. 721-740.
- Shock, E. L., and Helgeson, H. C., 1988, Calculation of the thermodynamic and transport properties of aqueous species at high pressures and temperatures: Correlation algorithms for ionic species and equation of state predictions to 5 kb and 1000°C: *Geochimica et Cosmochimica Acta*, v. 52, pp. 2009-2036.
- Shock, E. L., Sassani, D. C., Willis, M., and Sverjensky, D. A., 1997, Inorganic species in geologic fluids: Correlations among standard molal thermodynamic properties of aqueous ions and hydroxide complexes, *Geochimica et Cosmochimica Acta*, v. 61, no. 5, pp. 907-950.
- Sverjensky, D. A., Shock, E. L., and Helgeson, H. C., 1997, Prediction of the thermodynamic properties of aqueous metal complexes to 1000°C and 5 kb: *Geochimica et Cosmochimica Acta*, v. 61, pp. 1359-1412.
- Tanger, J. C., and Helgeson, H. C., 1988, Calculation of the thermodynamic and transport properties of aqueous species at high pressure and temperatures: Revised equations of state for the standard partial molal properties of ions and electrolyte: *American Journal of Science*, v. 288, pp. 19-98.